Studying marine fog using

the Weather Research and Forecast (WRF) model

Zheqi Chen

A Thesis submitted to The Faculty of Graduate Studies in partial fulfillment of

the requirements for the degree of

Master of Science

Graduate Program in Earth and Space Science and Engineering

York University

Toronto Ontario

April 2021

Abstract

Fog can seriously affect daily life. However, due to the complex mechanisms involved, accurate and in time fog forecasts are still difficult. This study has used the Weather Research and Forecast model (WRF) to simulate marine advection fog over Sable Island, NS in summer 2018. Chapter 2 uses the real case simulation to find a good physics parameterization and apply it as a daily forecast. The results show that the model tends to give much lower visibility than observations on this small offshore island. Chapter 3 uses the single column model to simulate an advection fog. Different gravitational settling options have been examined, and it is found that the turbulent deposition can be a good solution to the problem. In Chapter 4 the turbulent deposition is tested in the real case simulation. The results show that the visibility can become higher, but further study is needed.

Acknowledgements

First of all, I would like to thank my supervisors, Peter Taylor and Yongsheng Chen, for giving me the chance to participate in this research. They have been guiding me throughout my entire master's program.

I would also like to thank George Isaac, my committee member, and Li Cheng in our research group. They are very important in this research. This thesis cannot be finished if we are missing anyone.

Lastly, I cannot be more grateful to my parents and friends. It is impossible for me to study here without their support.

Table of Contents

List of Tables

List of Figures

Chapter 1

Introduction

1.1 Basic Background

Fog can seriously affect transportation and public safety. Driving in fog can be dangerous. Flights can be delayed or cancelled if fog appears. Inaccurate fog forecasts cost U.S. aviation up to $875 million in additional operational costs annually (Riordan and Hansen 2002). Therefore, accurate and in time forecasts of fog are essential to the economy, and public safety. However, forecasts of sea fog still suffer from the lack of observations over the open sea, parameterization uncertainties, and coarse vertical resolution in numerical models for representing boundary layer processes (Yang et al. 2018). In this thesis, the Weather Research and Forecast model (WRF) version 4.1.2 has been used to simulate fog over Sable Island, NS, in an attempt to test the accuracy of marine fog forecasting.

1.1.1 Sable Island

Sable Island (44˚N, 60˚W), shown in Fig. 1.1, and literally an “island of sand”, is a 30 km

long narrow (mostly < 1 km wide), crescent-shape sand bar in the Atlantic Ocean about 150 km offshore from Nova Scotia, Canada. It has some vegetation, cranberry bushes and grass, wild horses and many seals and is now a National Park, which must grant permission prior to any visit.

In the past it was the site of many shipwrecks and was known as the graveyard of the Atlantic, due to the frequent fog and sudden strong storms in the area. According to ECCC Climate Normals, averaged over 30 years (1971-2000), more than 200 hours of fog (visibility ≤ 1 km) per year have been observed in June and July on the island (Table 1.1), which is due to the contrasting effects of the cold Labrador Current and the warm Gulf Stream. On average there are 127 days out of the year that have at least 1 hour of fog.

Environment and Climate Change Canada (ECCC) operated an upper air station there for many years until it closed in August 2019, where radiosondes were carried aloft by hydrogen-filled weather balloons to altitudes beyond 40 km. Taylor et al. (1993) used the island as an offshore platform to study the surface features of offshore frontal passages in winter storms, and it would be an ideal location from which to study summer marine fog situations, since its long and narrow shape of land surface will have minimal impact.

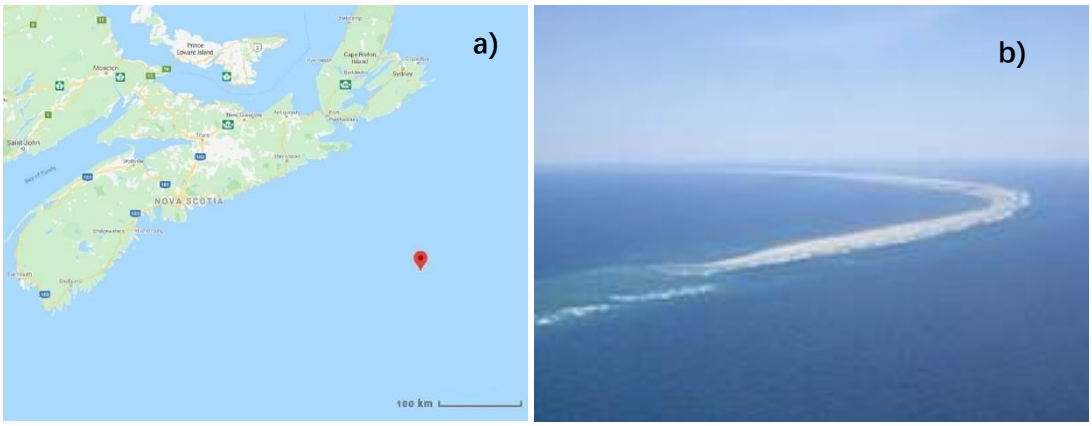

Figure 1.1 (a): Location of Sable Island (44˚N, 60˚W). (b): A photo of Sable Island (from https://en.wikipedia.org/wiki/Sable_Island).

Table 1.1 Yearly visibility information in hours from ECCC Sable Island station, averaged over 30 years (1971-2000). (from ECCC Climate Normals)

	Jan	Feb	Mar	Apr	May	Jun	Jul	Aug	Sep	Oct	Nov	Dec	Year
<1km	45.8	52.1	77	107.7	166.6	205.2	215.6	127.3	35.3	28.5	32.5	28.6	1122.1
1-9 km	179.9	147.8	140.3	158.1	158.8	153.2	183.7	175.7	122.1	106.9	132.5	144.1	1803
> 9km	518.3	477.8	526.7	454.2	418.6	361.6	344.8	441.1	562.6	608.6	555	571.4	5840.6

1.1.2 WRF

WRF is a next-generation mesoscale numerical weather prediction (NWP) system designed for both atmospheric research and operational forecasts. The model serves a wide range of meteorological applications across scales from tens of meters to thousands of kilometers. The real case simulation (em_real) and single column case (em_scm_xy) in WRF version 4.1.2 have been used for this study. For further details, readers can refer to Skamarock et al. (2019), the User's Guide and NCAR Technical Notes.

For the real case studies in this research, NCEP GDAS/FNL 0.25 Degree Global Tropospheric Analyses and Forecast Grids are used. They come from the Global Data Assimilation System, which continuously collects observational data from the Global Telecommunications System. This data set is on 0.25˚ by 0.25˚ grids prepared every 6 hours. It includes data at 26 mandatory pressure levels from 1000 hPa to 10 hPa, as well as at the surface. The parameters include surface pressure, sea level pressure, sea surface temperature, soil temperature and moisture, plus geopotential height, temperature, relative humidity, u and v winds, vertical motion and vorticity at multiple pressure levels.

For the idealized SCM studies, no external data are required, but an input sounding data set is created and the source code is modified, in order to allow vertical level to be specified, and to program the surface temperature to decrease over time.

The single column model which actually uses a 3x3 horizontal grid, provides a convenient tool for this research because compared to the real case simulation, it has far fewer grid points and requires much lower computational cost and time. Most simulations can be finished within 5 minutes. Also, its input data are easy to edit, not requiring external and real data, which allows the user to quickly get results with different initial and boundary conditions. In a real case simulation, the full physics package is working and it is difficult to focus on one particular part of the model, but the single column model is simple and it provides the option to turn off some of the mechanisms.

It is worth noting that the WRF model does not use the data directly as the initial condition. It has its own hydrostatically-balanced reference state, which is the initial

condition of a simulation. The provided data in the file called wrfinput will be used to compute the perturbations of the meteorological variables. As the simulation time goes forward, the model can adjust from the initial conditions to a state that is consistent with its own numerics and physics and to develop appropriate large-scale circulations. This is the so-called spin-up time. In terms of equations, the pressure can be expressed by $p = \bar{p}(\bar{z}) + p'$ where variables with an overbar is in the reference state and p' is the perturbation. The same equation is applied to other variables too. With calculations with smaller numbers, the results can be more precise and the truncation errors can be reduced (Skamarock et al. 2019). The spin-up time should be at least 12h and likely depends on the quality of the model input and the condition of the soil fields (Bonekamp et al. 2018). The SCM also has a spin-up time, but with much fewer grids the time is negligible.

After a simulation has finished, a file called wrfout with the starting time of the simulation will be created, which is in NetCDF format. There are a variety of methods to read the file and analyze the data. In this research, the NCAR Command Language (NCL) has been used.

NCL is an open source interpreted language designed specifically for scientific data analysis and visualization. It is a powerful language for reading, writing, manipulating and visualizing scientific data. It also provides specific functions for WRF data analysis, such as calculating variables like temperature or relative humidity that are not directly given in the WRF model output (wrf_tk, wrf_rh), finding the nearest longitude latitude location for a specified gird point (wrf_user_ij_to_ll), and interpolating data at a desired level

(wrf_user_intrp3d).

1.2 Theoretical Background

It is important to provide some background on the mechanisms involved in fog formation.

1.2.1 Marine Fog

In meteorological practice, fog is observed when the visibility, or the distance at which a reference object cannot be distinguished from its background, falls below 1 km. It is specifically associated with near-surface layers containing water droplets averaging 10-20 μm in diameter, in concentrations up to 1 g m^{-3} (de La Fuente et al. 2007).

Most fogs that occur over inland areas come from cooling of the surface by longwave radiation, which will usually dissipate in daytime when solar radiation heats the air. However, marine fog that occurs over the ocean and coastal regions can last for days (Table 1.1) and usually involves advection of warm, moist air over colder water. The difference between sea air temperature and sea surface temperature during advection fog is typically between 0.5 and 3 ˚C as the sea surface cools the near-surface air (Yang et al. 2018).

Wilson and Fovell (2018) addressed the importance of fog-top cooling in radiation fog. During the starting stage of a fog, the radiative flux divergence at the surface dominates the cooling process and supports the initial growth of fog droplets. Although various gases are able to absorb and emit the radiation, liquid water is more efficient. Therefore, as the fog

becomes thick enough, water droplets within the fog will absorb longwave radiation from the surface and emit in both upward and downward directions. Since radiation gets emitted back, the surface cooling will become weaker, while the cooling at the fog top with upwelling radiation will dominate the process. Such fog top cooling will generate turbulence at that level and will help the fog to grow thicker as well as to dissipate earlier.

It is suspected that the longwave radiation cooling is also important for advection fog. Observations with sea air temperature lower than sea surface temperature within a fog event have been reported. The classic view of sea surface cooling the air cannot explain such phenomenon, which implies other cooling mechanisms at work. Findlater et al. (1989) analyzed the heat budgets and found that the fog top cooling is balanced with the latent and sensible heat flux from sea surface after the formation of advection fog. Zhang and Ren (2010) suggested that the longwave radiation cooling at fog top contributes to the reversed air-surface temperature through turbulent mixing in the fog layer (Yang et al. 2018).

Kunkel (1984) had measurements of advection fog over land in July 1980 and July 1981, at 5 m and 30 m on a tower "in the middle of a large, flat, open area" about 12 km inland from the Atlantic on Cape Cod. With some variability his liquid water content values ($g\ m^{-3}$) are always higher at 30m than at 5m, with factors of 2-3. The results also showed that the daily mean concentration of droplets > 2.5 μm at 30 m was about 230 cm^{-3} and at 5 m the value was 65 cm^{-3}. For radiation fog, Pinnick et al. (1978) had measurements at multiple heights from February 1976, above an inland site in Germany. The land surface was also open and flat. The instruments were carried aloft by tethered balloon. The liquid water

content was calculated by droplet size distribution. In 3 of the 4 cases, the results show that liquid water increases with height, also with factors of 2-3 between the surface and 100 m.

For NWP models, the difficulty of fog forecasting comes from the fact that numerous feedbacks in fog can occur, all of which are sensitive to the resolution, initial conditions, and physical parameterizations within the model. Among the parameterizations, the land surface, microphysics, radiation, and boundary layer, each play particularly important roles during the formation, maintenance, and eventual demise of fog (Wilson and Fovell 2018). The opinion of Gultepe et al. (2006) is that "most NWP models were unable to provide accurate visibility forecasts, unless they accounted for both liquid water content and droplet number". Wilkinson et al. (2013) noted that at that time the UK Met Office Unified Model used "a taper curve for cloud droplet near the surface". They reduced the droplet numbers from the surface to 150 m without changing the liquid water concentration so that they could remove more liquid water from the lowest model levels. It seemed to work but certainly it is arbitrary and unphysical.

1.2.2 Planetary Boundary Layer (PBL)

Fog forms within the PBL, which makes it more difficult to forecast than cloud, although both result from water vapor condensation. Over land the PBL can respond to changes in surface radiative forcing in less than an hour, and the wind changes with height due to surface friction. Turbulence and vertical mixing of heat and moisture are important factors. After the lowest layers cool by conduction and may also accumulate water vapor evaporating from the

sea surface, turbulent mixing with cooler dryer air above may initiate a convective process sustained by latent heat release from droplet condensation. It is theorized that saturation and droplet condensation first occur at an inversion height then proceed towards the surface, suggesting a cloud formed initially would develop downwards to create a fog bank (de La Fuente et al. 2007).

Although each parameterization in the WRF model plays an important role in fog forecasting, the PBL scheme may be the most important one. Therefore, it is necessary to explain how the PBL scheme in a NWP model works.

The PBL scheme is responsible for vertical sub-grid-scale fluxes due to eddy transport in the whole atmospheric column, not just the boundary layer. Moisture, heat and momentum will be exchanged through the eddies. Such eddies operate on spatiotemporal scales that cannot be explicitly represented on grid scales. Firstly the surface fluxes are provided by the surface layer and land-surface schemes, then the PBL scheme will determine the flux profiles within the well-mixed boundary layer and the stable layer, and thus provide atmospheric tendencies of temperature, moisture and horizonal momentum in the entire atmospheric column.

There are two major components in the process of representing the turbulence mathematically: the order of turbulence closure and whether a local or nonlocal approach is employed.

In a turbulent flow, the variables in the equations of motion are described with mean and fluctuation components. The mean component represents the time-average conditions of

the background atmosphere, while the fluctuation term represents the deviations from the background mean state. With such decomposition and after time or ensemble averaging, mathematically the equations of motion always contain more unknown terms than known terms, where the unknown terms, like w'T' the vertical heat flux, are typically an order higher than the other terms like vertical wind w and temperature T, which leads to the closure problem. Therefore, a nth-order closure scheme will empirically relate the unknown terms of moment n+1 to lower moment known terms, where n is an integer, typically 1 or 2. Some schemes however have 1.5-order closure, meaning that they will predict 2nd-order fluxes and turbulent kinetic energy (TKE) by diagnosing 2nd-order moments for some variables (Cohen et al. 2015).

The second component is whether to use a local or nonlocal gradient approach. In a local scheme, only those vertical levels that are directly adjacent to a given point directly affect variable gradients at the given point. On the other hand, multiple vertical levels can be used to determine fluxes at a given point in a nonlocal scheme. Therefore, a local scheme may have a disadvantage if nonlocal approach can represent fluxes in a deep PBL more realistically.

For the two main PBL schemes in this study, the Mellor-Yamada Nakanishi Niino (MYNN) Level 2.5 scheme (Nakanishi and Niino, 2006 and 2009) is a local, 1.5-order closure scheme. The Yonsei University (YSU) scheme (Hong et al. 2006) is a nonlocal, 1st-order scheme.

Some PBL schemes will have a specification of the surface layer scheme, which

shows the deep connection of the two parameters. The YSU PBL scheme can only be used with revised MM5 Monin-Obukhov scheme (Jiménez et al. 2012) (sf_sfclay_physics = 1). The MYNN PBL scheme is compatible with the above MM5 scheme, but also the Monin-Obukhov (Janjic) scheme (sf_sfclay_physics = 2) and the MYNN surface scheme (sf_sfclay_physics = 5). This study will focus on the MM5 and the MYNN surface scheme, option 1 and 5 respectively.

Not many descriptions for the MYNN surface scheme are available. It computes the surface stability parameter z/L, transfer coefficients, and the momentum and scalar fluxes over land, water, and snow grid points. However, if a land surface model is used, the scalar fluxes will be recalculated by the land surface model. The PBL scheme will take the following variables from the surface scheme: u* the friction velocity, HFX the heat flux, QFX the water vapor flux and z/L. The first three are used for calculations like the lower boundary conditions or initializing the parcels for the mass flux scheme. The surface stability parameter z/L is used for computing the surface layer length scale (Olson et al. 2019).

A number of references on the MM5 similarity scheme is available on the WRF reference page (https://www2.mmm.ucar.edu/wrf/users/physics/phys_references.html). The old MM5 scheme is kept as option 91. The new version of option 1 is the revised MM5 scheme from Jimenez et al. (2012). Compared to the old version, it provides a self-consistent formulation valid for the full range of atmospheric stabilities, which gives a shaper afternoon transition. It also has an overall improvement in the estimation of typical near-surface meteorological variables in terms of diurnal amplitude, especially 2 m temperature.

Chapter 2

Real Case Simulation

In the real case study, 2 experiments have been done. The object of the first experiment is to find good domains and physical parameterization options within WRF for fog simulation. The second experiment will use the setting to do daily simulations to examine the performance of the WRF model.

Two nested domains are used, a small and relatively high-resolution domain with dx = 10 km (181 x 181 points) inside a domain of dx = 30 km (120 x 100 points) (Fig. 2.1a) The large domain 1 is appropriate since it captures the fog in the surrounding area (Fig. 2.1c). The Grand Bank area in the North Atlantic Ocean is also a location to study marine fog. In the summer of 1913, Taylor (1917) took 806 observations with kites on a ship, with 141 times in fog. He concluded that fog in the area mainly formed as warm air from the Gulf Stream flowed over the cold water of the Grand Banks. More recently, Issac et al. (2020) used observation data from 1997 to 2017, at a platform at 69m above sea level, and a buoy on the ocean. Besides the source of the warm air, they also found that a air temperature 2 °C warmer than the sea surface temperature would be important. Considering the possibility of a future

study in this area, domain 2 is adjusted so that it includes both Sable Island and the Grand Bank area for convenience. In the vertical, 37 vertical levels are used, with 14 levels lower than 1 km. A sigma coordinate and staggered grid are used. The lowest model sigma levels are 1.000, 0.996, 0.993, 0.988, 0.983, 0.976, 0.970, 0.962, 0.954, 0.944, 0.934, 0.922, 0.909 and 0.804. The lowest diagnostic levels are 2 m for liquid water content, water vapour and temperature and 10 m for wind speed above the surface. At this resolution, the grid point of Sable Island (i=62, j=51) is treated as water surface (Fig 2.1b).

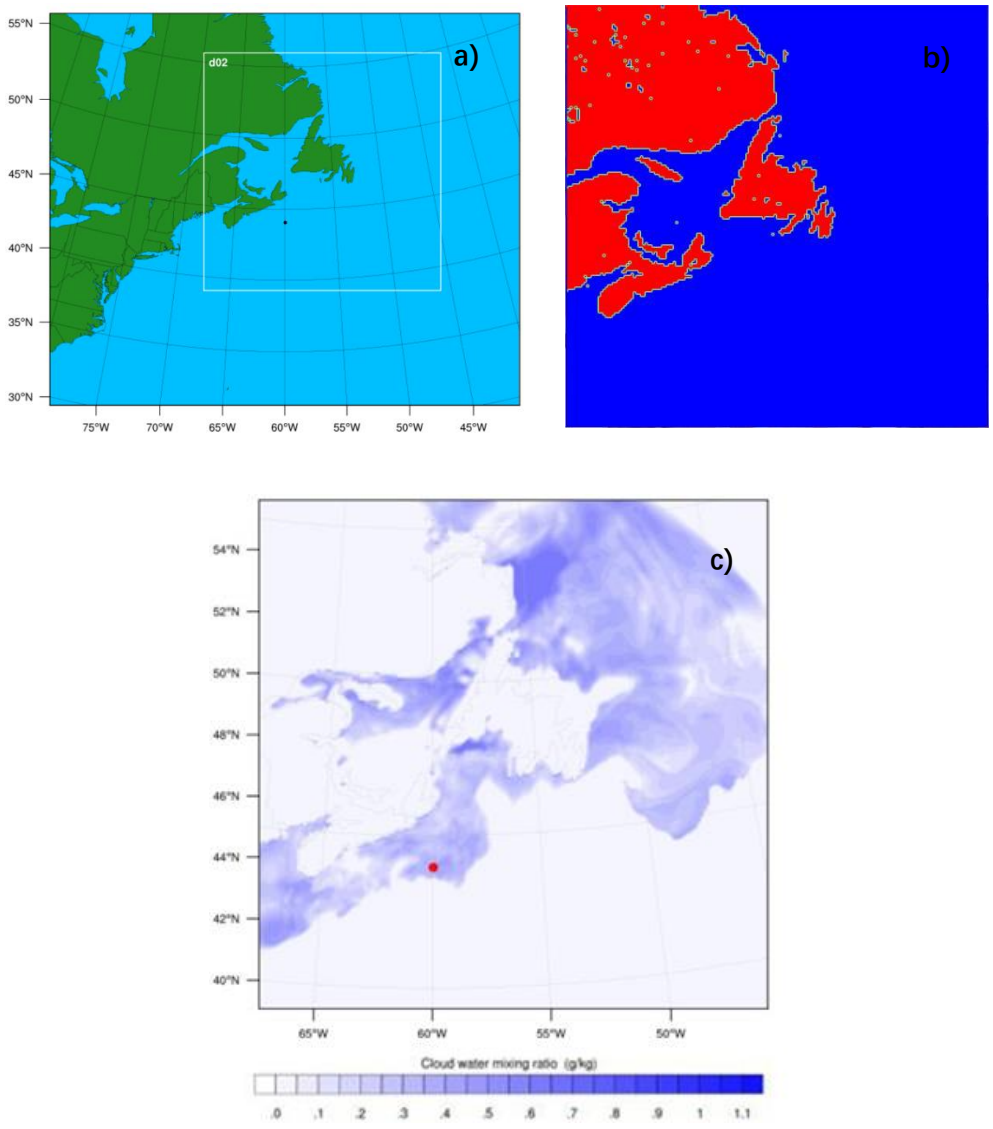

Figure 2.1 (a): WRF model domains. The whole area is the larger domain 1. The square with white border is the smaller domain 2, and the black dot is the location of Sable Island. (b): Landmask in domain 2. The grid point of Sable Island is on the water surface. (c): One moment of the smaller domain with cloud water. The red dot is Sable Island.

2.1 Experiment 1

2.1.1 Experiment Set Up

In the first experiment, different physics parameterizations are examined based on a 3-day period, August 14 12Z to 17 12Z, 2018, when a long fog event occurred, according to ECCC historical weather reports.

The following physics schemes have been selected, and combinations of them, a total of 22 cases, are all run for the same period. Lin et al. (2017) showed that a combination of the Thompson microphysics scheme (Thompson et al. 2008), and the RRTMG radiative scheme (Iacono et al. 2008) predicts fog duration comparable with the observations, so most cases are done with the Thompson microphysics scheme. Therefore, the number of combinations is less than $3^4 = 81$.

Some of the PBL and surface schemes are introduced in 1.2.2. Thompson microphysics scheme is a bulk scheme which treats the size distribution of hydrometeors as an empirical function. It uses a generalized gamma distribution for water species. It predicts the mixing ratios of five species: cloud water, rain, cloud ice, snow and graupel, and it also predicts the number concentration of cloud ice (second-order).

Table 2.1 Chosen WRF physics parameterizations. For each parameter, a scheme can be selected. The combinations of each of them are examined. References of the schemes can be found on https://www2.mmm.ucar.edu/wrf/users/physics/phys_references.html.

Parameters	**Schemes**
Planetary Boundary Layer	YSU (Yonsei University), MYJ, MYNN 2.5 Level TKE (Mellor-Yamada Nakanishi Niino)
Microphysics	Thompson, Lin, WSM (WRF Single Moment), WDM (WRF Double Moment)
Longwave/Shortwave	New Goddard, RRTMG (Rapid Radiative Transfer Model for General Circulation Models)
Surface Layer	Revised MM5, Janjic, MYNN surface layer

2.1.2 Results

The QCLOUD (cloud water mixing ratio) values at the Sable Island grid point (62, 51) for each simulation have been compared (Fig. 2.2) to the fog period of the ECCC reports, in order to find a good setting for fog prediction. It is worth noting that although fog is defined as visibility lower than 1 km, sometimes ECCC will still report “fog” for weather even if the visibility is higher than 1 km. Since 1994, forward scatter sensors have been used on Sable Island, which is set at 2.5 m facing down at 45 degrees to give a visibility of 2 m, and there is also a real-time camera for the observers, so daytime visibility less than 1 km can be determined by human eyes. Using two methods may be the reason for such inconsistency between weather condition and the value of visibility. In this experiment, the period indicated is when the weather is reported as “fog”, rather than visibility lower than 1 km. Values in the output are only considered as QCLOUD = 0 or non-0. When there is a non-0 cloud water mixing ratio at low heights, we interpret it as meaning that fog occurs in the model. Then the period of the fog in the model is compared to the fog in the ECCC report.

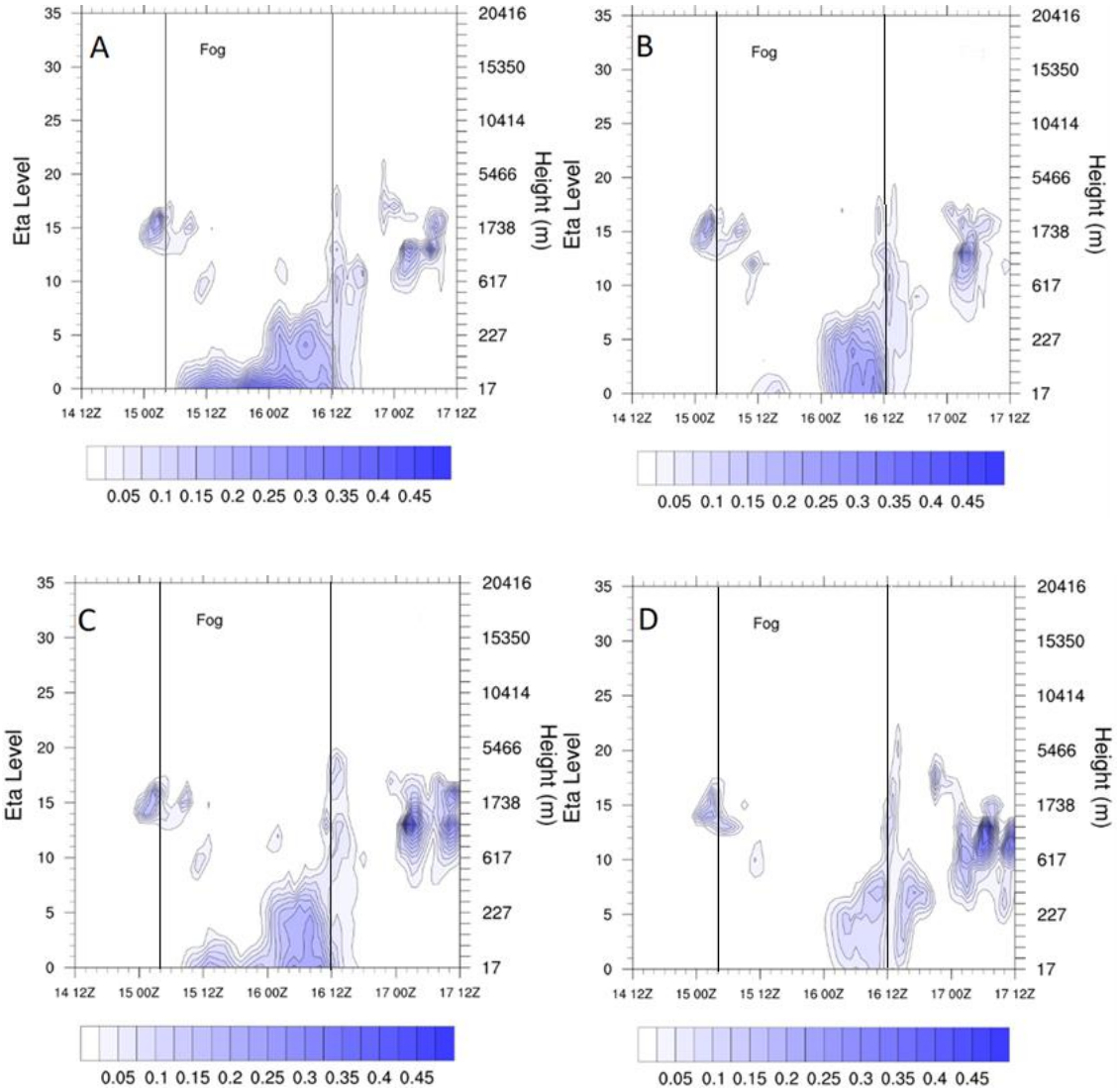

Figure 2.2 QCLOUD ($g\ kg^{-1}$) plots at (62, 51) from two different simulations (August 14-17, 2018). See text for explanation. The vertical lines correspond to ECCC reports with fog weather at Sable Island, from August 15 04Z to 16 00Z. Values are extracted from each vertical level, which is the left y-axis. The height is provided for reference as the right y-axis. The colour scale shows the value of QCLOUD.

Fig. 2.2 shows 4 example cases in this experiment. They all have the RRTMG radiation scheme and the Thompson microphysics scheme. Case A has the following schemes: YSU PBL and MM5 surface. Case B has MYNN PBL and Janjic surface. Case C has MYNN PBL and MYNN surface. Case D has MYJ PBL and Janjic surface.

We only consider the fog coverage time at the first model level. Case B and D should not be considered. Case A and C have very close coverages. Case A has two more hours within the "fog" period, but it also has two more hours outside the period, than Case C. Given that the WRF model tends to give too much liquid water, as in Chen et al. (2020), Case C would be a more cautious approach. Table 2.2 shows the detail of the physics settings of Case C:

Table 2.2 WRF physics parameterizations to be used in Experiment 2.

Parameter	**Scheme**	**WRF option**
Planetary Boundary Layer	MYNN 2.5 Level TKE	bl_pbl_physics= 5
Microphysics	Thompson	mp_physics= 8
Longwave	RRTMG	ra_lw_physics= 4
Shortwave	RRTMG	ra_sw_physics= 4
Surface Layer	MYNN	sf_sfclay_physics= 5

2.2 Experiment 2

2.2.1 Experiment Set Up

A long-term simulation has been performed with the setting above, which covers June, July, and August 2018. To simulate a daily forecast, each run is 36 h long, from 12:00 to 24:00 UTC on the next day, but the results of the first 12 hours from each run are discarded, for the reason of spin-up time. The visibility, wind speed and direction are compared to hourly ECCC reports.

There are no visibility values directly given in the WRF output. Two algorithms of visibility calculation were used. Since the maximum value in ECCC reports is 16.1 km, the maximum in calculation is set to be the same value. The first estimate is calculated by the formula (Isaac et al. 2020):

$$Vis = \frac{1.24{\rho_w}^{2/3}}{LWC^{2/3}N^{1/3}} \quad (2.1)$$

where $\rho_w = 1000kg\ m^{-3}$ is the density of liquid water, LWC is the cloud liquid water content in $kg\ m^{-3}$ and N is the number density of droplets which is set as a constant of $10^8\ m^{-3}$. This number of N is the default valued used in the Thompson microphysics scheme as droplet concentration for clean air over marine regions (Thompson et al. 2008). To get the liquid water content, the QCLOUD value, kg of water per kg of air, in the model output is used. Pressure and virtual temperature are extracted from the output first, then air density is calculated by ideal gas law $p = \rho R_* T_v$. LWC can be calculated by multiplying QCLOUD by air density.

Isaac et al. (2020) claimed that this algorithm only works for daytime visibility. In

nighttime when background light is important for human observers it is not valid. However as mentioned in 2.1.2, there is a forward scatter sensor in the year of 2018, which should be used in nighttime. The forward scatter sensor emits a beam from the transmitter to the receiver. When there are liquid water droplets, or anything that scatter light, some of the beam light is scattered and lost. By calculating the difference between emitted and received light, the instrument can give the value of visibility. Therefore, nighttime visibility should not be a problem and we will use this formula for the whole period.

The algorithm has some other limitations. It only considers fog, that is visibility lower than 1 km, but not haze or mist that are less dense with visibility higher than 1 km. In addition, it only considers visibility reduced due to fog droplets, but not rain water or other hydro species. Therefore, we should have these in mind when analyzing the data.

The second visibility option is the GSD algorithm used in NCEP's Unified Post Processor (UPP) version 2.2 (Lin et al. 2017). This algorithm compares the visibility due to relative humidity and the visibility due to hydrometeors, and uses the minimum. In the original algorithm, the visibility due to hydrometeors includes 5 species, but in this research, only cloud water and rainwater are considered in the calculation, since there was no snow or graupel weather in the summer of 2018. Cloud ice may exist in the upper cloud but not near surface.

The visibility due to relative humidity is calculated as

$$Vis_{rh} = 60 * \exp(-2.5 * q_{rh}) \tag{2.2}$$

where $q_{rh} = \min(0.8, (rh_{max}/100 - 0.15))$, rh_{max} is the maximum relative humidity at

the lowest two model levels.

The visibility due to hydrometeors is calculated as

$$Vis_{hydro} = \min(90, -\ln(0.02)/(\beta + \beta_0)) \quad (2.3)$$

where $\beta = \beta_{cw} + \beta_{rw} + 1e^{-10}$, $\beta_{cw} = 144.7C_{cw}^{0.88}$, and $\beta_{rw} = 2.24C_{rw}^{0.75}$. β is the extinction coefficient for each species, associated with mass concentration ($g\ m^{-3}$) of cloud liquid water C_{cw} and rain water C_{rw}. β_0 is the extinction coefficient of aerosol, but neither Lin et al. (2017) nor the source code of UPP v2.2 mentions the value of it. Therefore, it is treated as 0 in the calculation.

2.2.2 Results

Visibility

The correlation plots between model visibility at the first model level (17 m) and reported visibility (2m) on Sable Island are shown in Fig. 2.3. A total of 2206 hours are plotted, a little less than 92 days x 24 hours since the observations for 2 hours are missing. The first plot of Fig. 2.3 uses an algorithm from Isaac et al. (2020). From the first panel, the overview, one can see that the correlation is not good. When the observation reports a visibility lower than 5km, it means that fog or mist (1-2 km) or haze (2-5 km) is observed, but the model predicts visibility lower than 2 km for most of the cases. This is the reason why those data points lay along the x axis. Many data points are near the top left corner, meaning that the fog is missed by the model prediction. The reason why all the misses are

at 16.1 km is that when QCLOUD = 0 in the model, the Isaac's formula will be divided by 0, so the maximum value is given as 16.1 km instead, which is the maximum value of the ECCC report. After the plot is zoomed in to visibility values below 1 km, the correlation is still not good. From the scale, green colour means there are 10-80 data points in this range, and blue means the number is less than 10. Therefore, one can see that many data points are at the value when the observed visibility is from 0.2 to 0.5 km, the model visibility is at 0.05 km. The WRF model predicts much lower visibility than the observation.

The second plot of Fig. 2.3 uses the GSD visibility algorithm. From the first panel, since it takes the minimum of the two calculations, the plot is separated by model visibility of 8 km, which is certainly unphysical. The same problem remains when visibility is lower than 1km, that the model visibility is still much lower than the observed visibility when QCLOUD appears in the model.

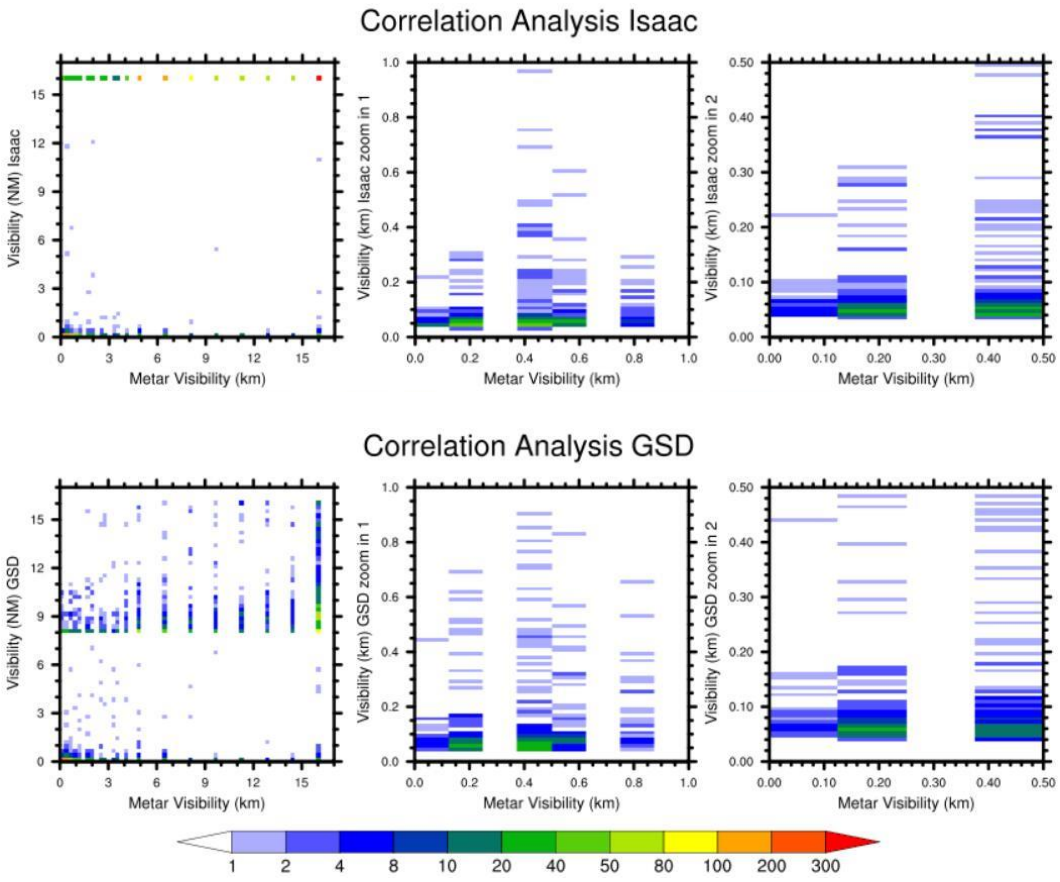

Figure 2.3 Correlation plots of visibility using the two algorithms. Isaac et al (2020) and GSD in UPP. The colour is the number of data points at this value.

Table 2.3 Numbers of hit, miss, false alarm, correct negative and threat score from the two algorithms. Definitions are in the text.

	Hit	Miss	False Alarm	Correct Negative	Threat Score
Isaac et al.(2020)	395	145	336	1330	0.451
GSD	390	150	327	1339	0.450

Table 2.3 summarizes the numbers in the four conditions: hit, miss, false alarm and correct negative, defined by visibility ≤ 1 km in both model and observation, visibility ≤ 1km in model but > 1km in observation, visibility > 1km in model but ≤ 1km in observation, and visibility > 1km in both, respectively. The threat score is also listed, calculated by hit/(hit+miss+false alarm).

Although the two algorithms have some difference, the two give very close numbers in all the four conditions. Therefore, the assumption that nighttime visibility is not a problem is correct. Also, the low visibility in both calculations should come from the amount of cloud water, rather than rain water. The cloud water mixing ratio should be higher than the observation, and this has been mentioned in Chen et al. (2020).

From Fig. 2.3, it is noticed that some data are located in the range of 1-3 km in observation, but the model visibility is also low. Table 2.4 summarize the four conditions with threat score with the threshold of 3 km.

Table 2.4 Numbers of hit, miss, false alarm, correct negative and threat score from the two algorithms, with threshold of 3 km.

	Hit	Miss	False Alarm	Correct Negative	Threat Score
Isaac et al.(2020)	531	283	208	1184	0.520
GSD	528	286	206	1186	0.518

If we include conditions with less dense fog, the model seems to work better, based on the threat score. The model catches some of these hours and produces liquid water rather than a miss. However, the amount of cloud water is still too high.

Wind

The correlations between model wind speed and direction and the reported wind, both at 10m, are good (Fig. 2.4). With 56 hours of observation missing, a total of 2149 hours of data are compared. Note that observation of wind direction is in 10 degree bins, and wind speed is reported by ECCC in km h^{-1} with no decimal place. Since marine observations are generally reported in knots we do the same here. Because some numbers do not appear in the report, such as 10, 12, 14 km h^{-1}, gaps are shown in the plot. Fig. 2.4 shows that the winds frequently come from the SW direction. The mean wind speed of observations is 10.38 knot, but the model has mean wind speed of 11.14 knot. Some differences in wind speed are noticed. Therefore, situations with fog and without fog are separated in Table 2.5.

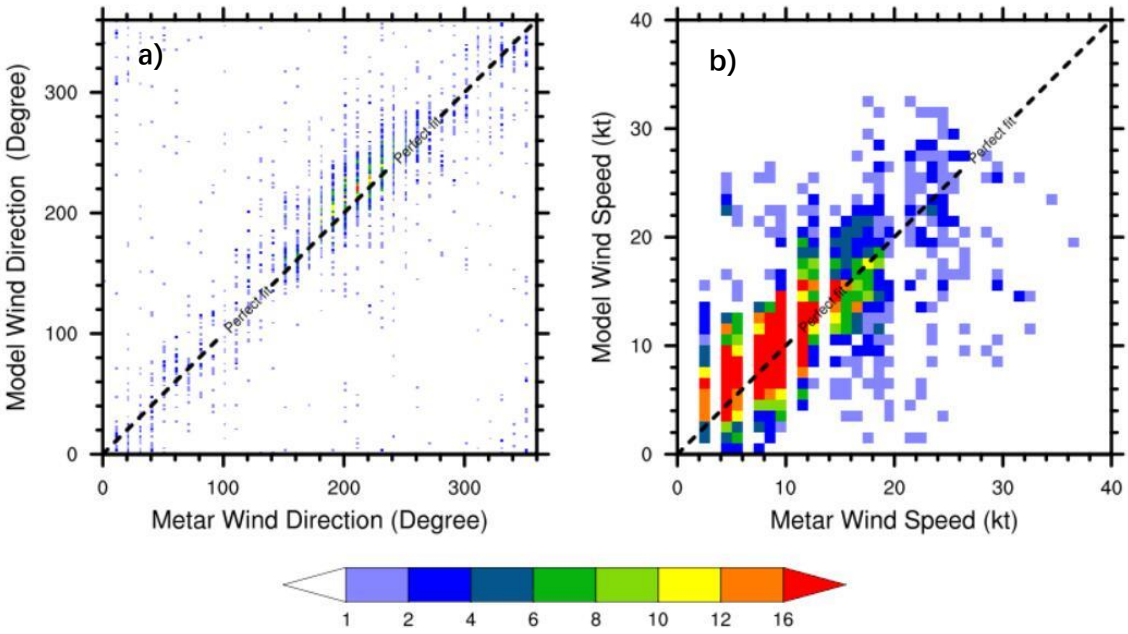

Figure 2.4 Correlations of wind direction (a) and wind speed (b). For wind speed the colour code is the number of occurrences in each 1 kt x 1 kt bin.

Table 2.5 Observed and model wind speed in different cases. Model visibility is calculated using Isaac's algorithm.

	Observed Wind Speed (knot)	**Model Wind Speed (knot)**
All Cases	10.38	11.14
Observed Visibility ≤ 1 km	9.47	10.28
Observed Visibility > 1 km	10.59	11.36
Model Visibility ≤ 1 km	9.68	10.09
Model Visibility > 1 km	10.62	11.60

From Table 2.5, in all situations, average model wind speed is higher than observed wind speed. The observed wind speeds are measures at a mast on the island, about 1 km inland from the water so some reduction in wind speed is to be expected. When fog occurs, either in the observation or the model, the mean wind speed of both is lower. A lower-than-normal wind speed may be helpful to the formation of fog.

Fig. 2.5 shows the wind roses in the different situations. When there is no fog in the observation, there are some winds in the NE direction, which is rare during fog events. Observed winds during fog events are concentrated in 200 and 210 degree bands. Model winds when fog is in the model are more averaged in the 225 degree band. When there is no fog in the observation, there are some winds coming from the south, but there is less south wind in the model when model visibility > 1 km.

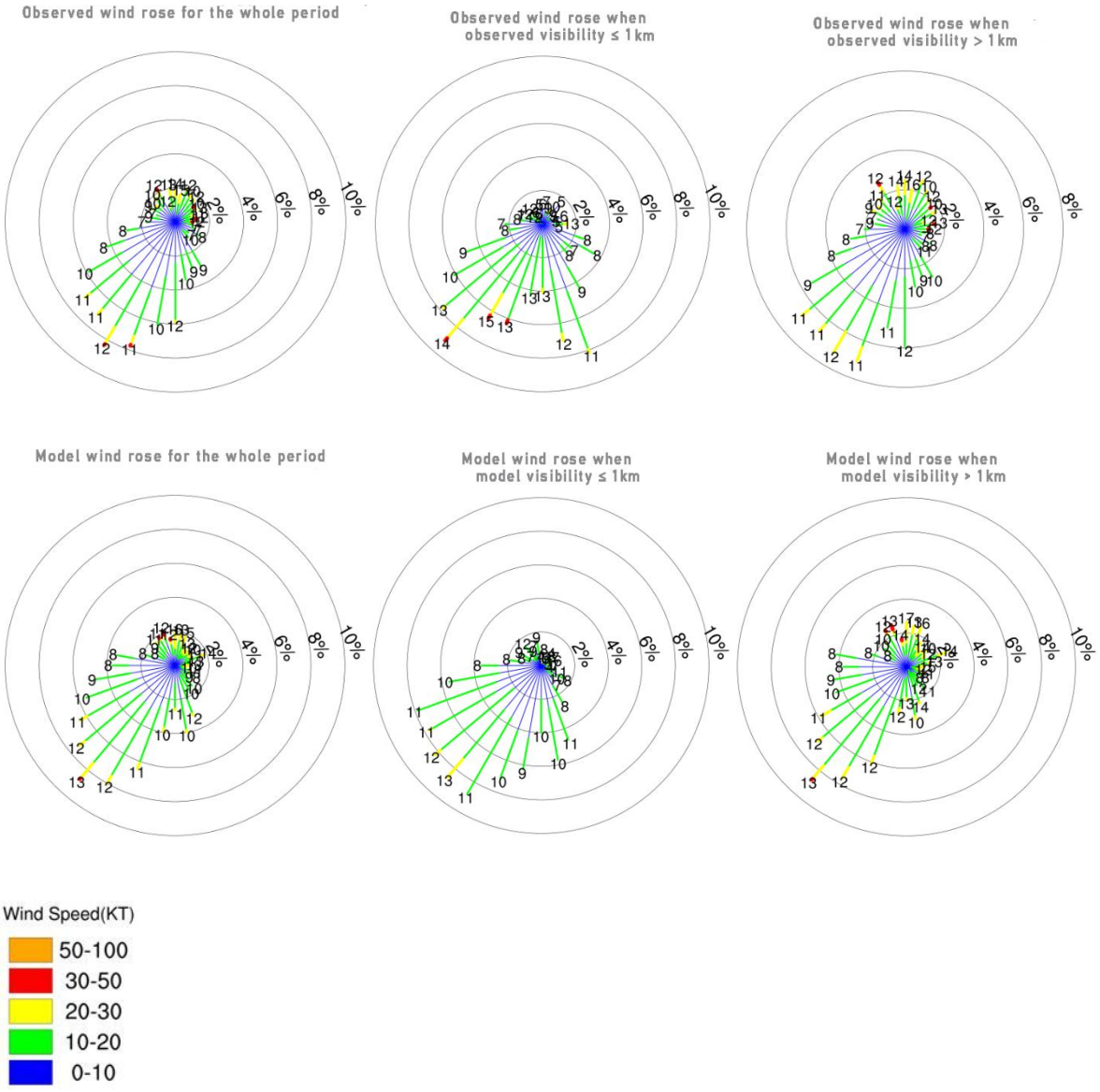

Figure 2.5 Wind roses in different situations. The numbers at the end of the bars are the average wind speed in the direction. The length of the bars shows the frequency of data from this direction in total of the data in this situation. Total numbers are indicated in the text.

Temperature

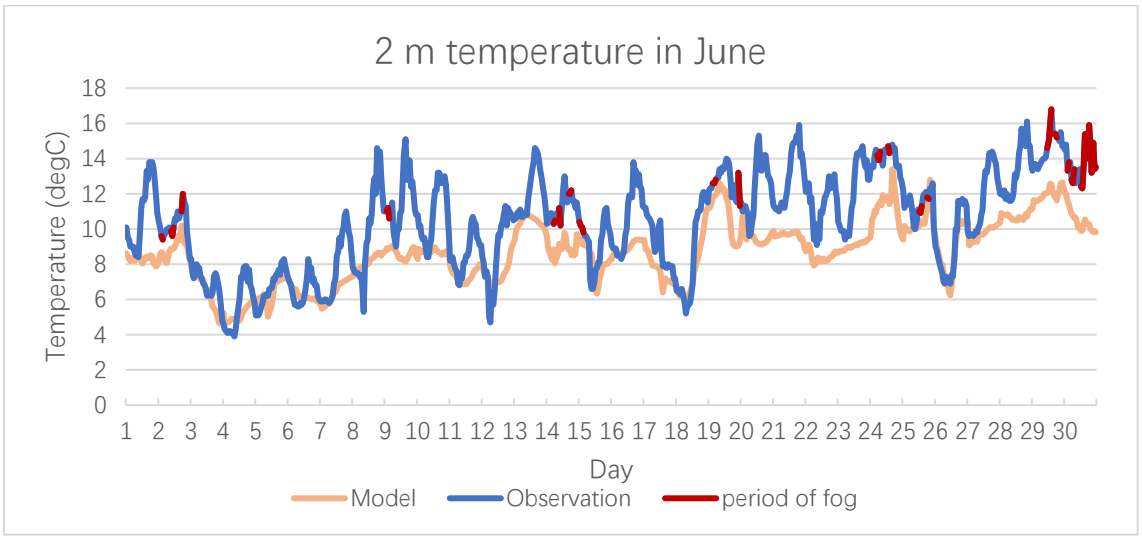

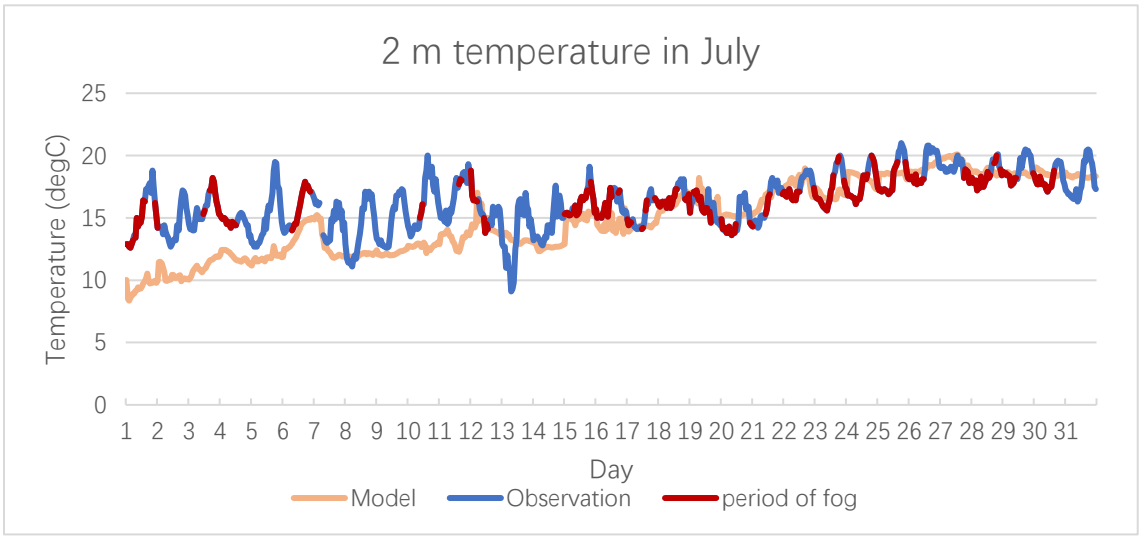

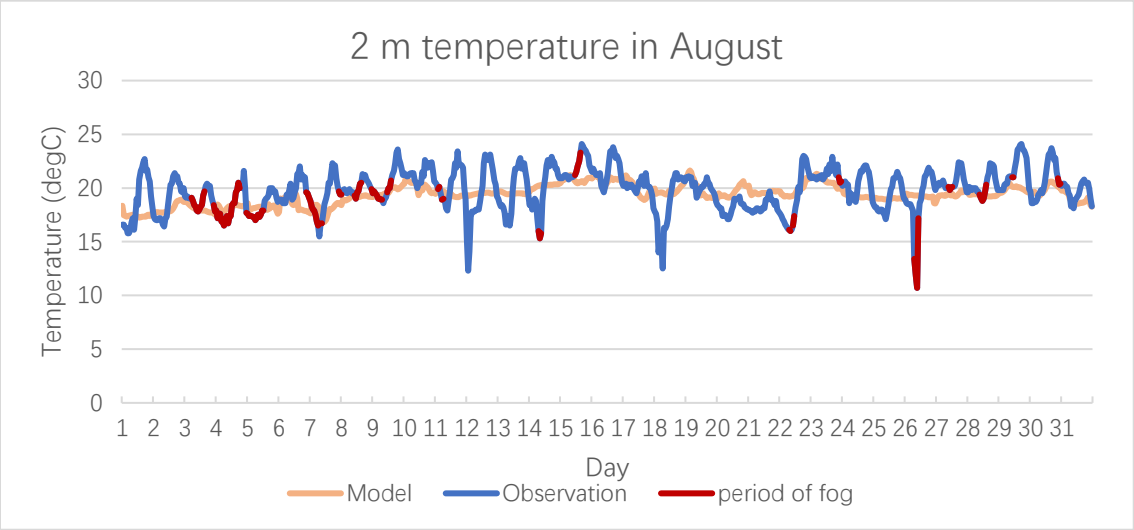

Figure 2.6 2m temperature time series from model and observation in June, July and August 2018. Two hours of observation in July are missing. The red part of the observation curve shows the period when observed visibility ≤ 1 km.

The Environment Canada weather station is in a more central location on Sable Island and this will have impacts on the measurements made, especially of temperature, but also wind speed. As mentioned above, the wind speed measurements are slightly lower than the model predictions in Fig. 2.4. Over water, observations in Isaac et al. (2020) at the Grand Bank area show very little diurnal variation in air temperature, and our WRF model results confirm this (Fig. 2.6). The METAR reports however do show a diurnal cycle with daytime temperature maxima typically 2-4 °C higher than night-time minima. A diurnal cycle will clearly impact relative humidity values since temperature affects saturation vapor mixing ratio, but with moderate wind speeds we can expect less variation in water vapour mixing ratio coming from the surrounding sea surface. The average observed 2 m temperature is higher than model temperature. After the middle of July, with a large number of fogs following, the two

temperatures start to get closer. It may show that more heat is transferred to latent heat rather than sensible heat. Therefore, the time series of water vapour mixing ratio are shown below.

Water Vapor Mixing Ratio

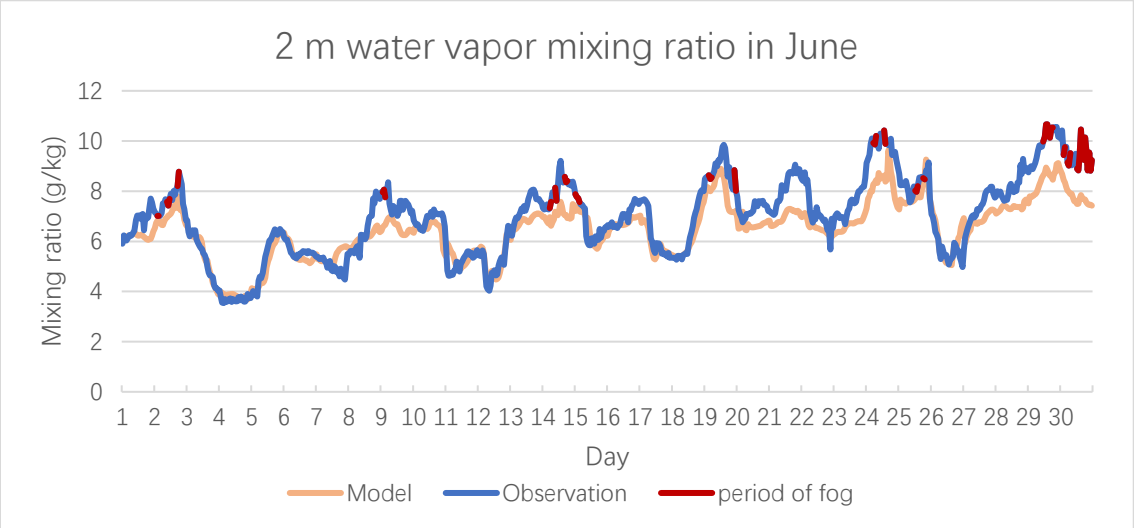

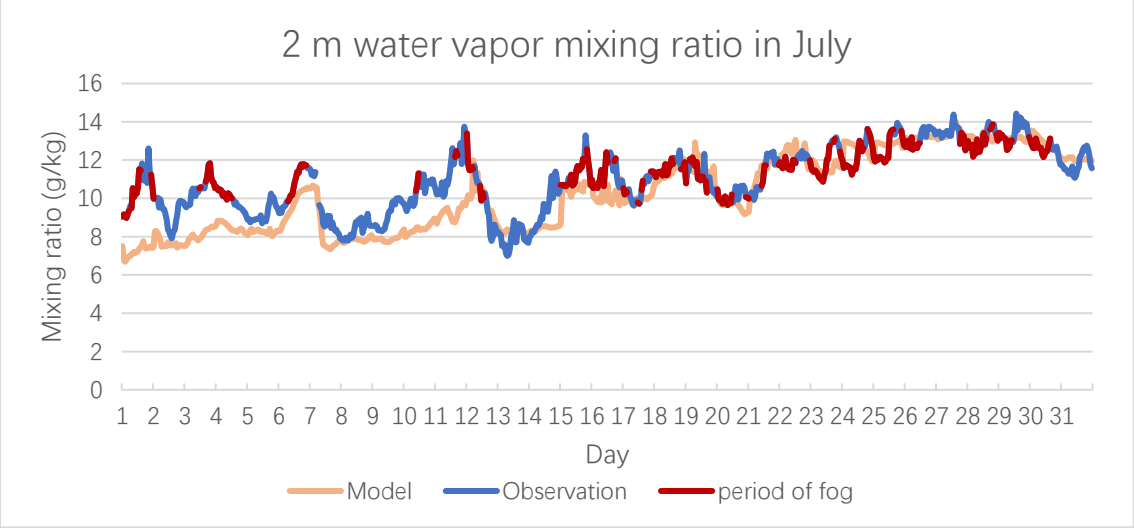

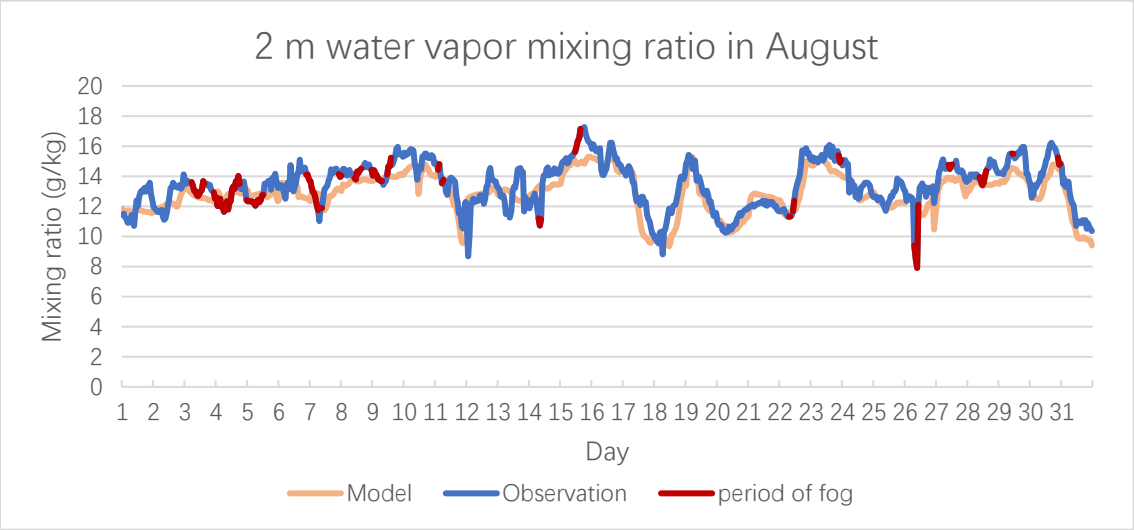

Figure 2.7 Water vapor mixing ratio from model and observation in June, July and August 2018. Two hours of observation in July are missing. The red part of the observation curve shows the period when observed visibility ≤ 1 km.

The ECCC reports only gives dew point temperature, therefore, the observed value in Fig. 2.7 is calculated by w=622*(e/(P-e)), where $e = 0.61 * \exp(17.27 * T_d/(237.3 + T_d))$ calculated by Tetens equation (Monteith and Unsworth 2008). Compared to 2 m temperature, vapor mixing ratio has a better fit, especially in June. The vapor mixing ratio is increasing with time within the 3 months. In the two experiments in this chapter, there was no land surface at our Sable Island location since there is no land surface grid point in our 10 km resolution model runs. This is the reason why in Fig. 2.6 the observed temperature is higher than the simulation and also that the model temperature does not have a strong diurnal cycle, while water vapor mixing ratio has smaller errors. The impact of land surface will be discussed in Appendix A.

2.3 Discussion

In this chapter, the real case simulation within WRF is used to simulate the fog over Sable Island. Two experiments have been done in this chapter. They both use the same two domains to cover the area, and the grid point of Sable Island is treated as a water surface. In the first experiment, different physics parameterizations have been used to do a 3-day simulation. We decided to use the setting in Table 2.2 to do an experiment with a longer period. In the second experiment, runs of 36 hours, with the first 12 hours discarded as spin-up time, are done to simulate the daily forecasts for June, July and August 2018. We have compared the results to the ECCC hourly reports. Two algorithms, Isaac et al. (2020) and GSD within the UPP software, are used to calculate the visibility. Both show that when the model catches the fog in the observation, the visibility is much lower. Wind simulations are relatively good, but the model wind speed is higher than the observation. Because the grid point in the model is a water surface, the 2 m temperature is relatively constant, without the diurnal cycle seen from the observations. 2 m vapor mixing ratio has a good match, showing that the model correctly predicts the movement of water vapor from the surrounding area. These factors do not seem to cause the model to falsely give that much liquid water. Therefore, in the next chapter, the single column model within WRF is used to take a more detailed look in the fog.

Chapter 3

Single Column Model (SCM)

3.1 Experiment Set Up

In order to run the SCM, a vertical profile with height, u-wind, v-wind, potential temperature and water vapor mixing ratio, with the surface pressure should be provided as the initial condition, which should cover the whole atmosphere in the model. The model top in this SCM study is 12 km.

To get the height profile, we firstly used the set of eta values with 37 levels, which is used in the real case simulation, to do an ideal case simulation. The height profile of the 37 levels from the result is then used for the input sounding. Values of the eta levels are a series of numbers decreasing from 1 to 0, with 1 being the surface and 0 being the top of the atmosphere. Therefore, although the eta values used are the same in the real case and this ideal case runs, with a different top in the 2 cases, the heights (z) are different. The real case simulation has a model top of 5000 Pa, while the SCM by default has the model top of 12000 m. Also, the standard SCM calculates eta values using top and surface pressure by default, but the code in module_initialize_scm_xy can be modified in order to allow the model to use

given eta values provided in the namelist file instead.

In our cases the surface potential temperature is set to be 300K, increasing by 4K/1000m with height in the atmosphere. Originally a neutral profile with 300K in the whole atmosphere was used for simplification, but it was found that a fog is easier to form in the current profile. The wind profile is generated with the following method: Firstly U=20m/s, V=0m/s is set for the whole column, with potential temperature = 300 K in the whole air column and no surface cooling. Vapor mixing ratio is 0 in the whole column. This simulation is run for 10 days, after which the atmosphere will reach a steady state. The u and v wind profiles at the last time step are then used in the input sounding for the research simulations.

The water mixing ratio profile is decided by the relative humidity first. Saturation vapor mixing ratio can be calculated by temperature and pressure, and it is multiplied by the desired relative humidity to get the vapor mixing ratio. In our case the air at the surface has a relative humidity of 100%, which decreases linearly with height. Our input sounding is in Table 3.1.

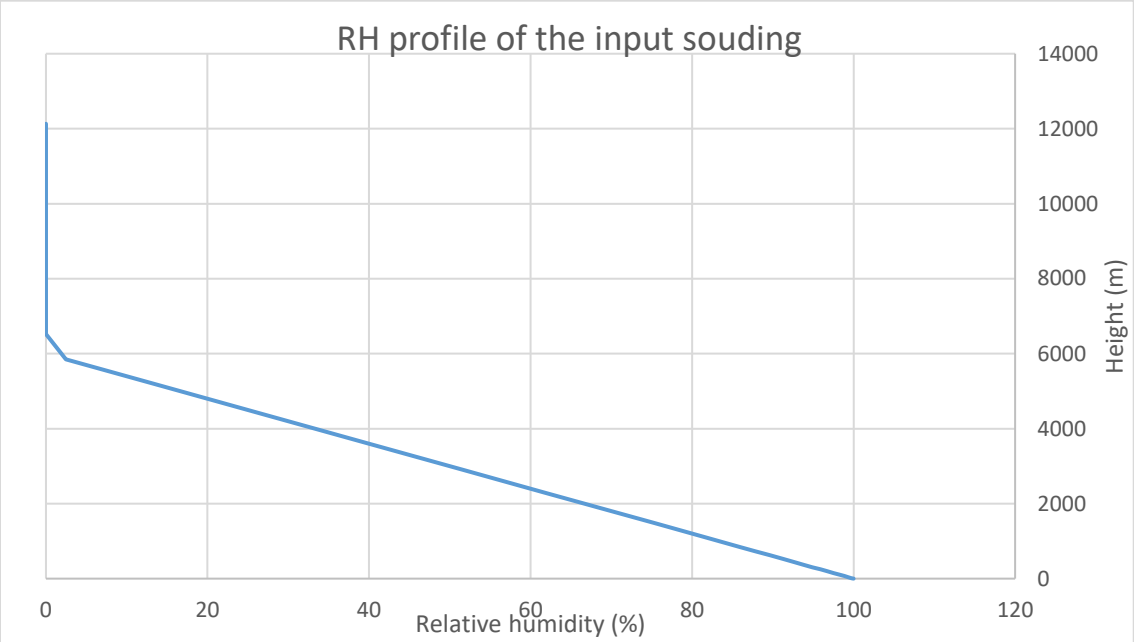

Figure 3.1 Profile of relative humidity that are used in the calculation of QV.

Table 3.1 Vertical profile used in input_sounding file. PSFC is the surface pressure so only the first row has a value.

z(m)	U (m/s)	V (m/s)	Theta (K)	Qv (kg/kg)	psurf (Pa)
0	0	0	300	0.021985	100000
14.36386	15.66428	1.734882	300.057455	0.021861	
39.51661	16.46412	1.795376	300.158066	0.021646	
68.32745	16.91014	1.821371	300.27331	0.021402	
104.4252	17.33809	1.834659	300.417701	0.021099	
147.903	17.6819	1.836351	300.591612	0.020738	
195.1703	17.95195	1.828004	300.780681	0.020351	
246.326	18.13941	1.816244	300.985304	0.019938	
305.0642	18.34531	1.79469	301.220257	0.019471	
371.5457	18.59395	1.757789	301.486183	0.018953	
445.8617	18.94404	1.687326	301.783447	0.018386	
528.2252	19.27828	1.604498	302.112901	0.017772	
622.5799	19.60619	1.510228	302.49032	0.017088	
729.2806	19.82945	1.437	302.917122	0.016337	
840.8768	19.99547	1.367795	303.363507	0.015578	
1086.145	20.18544	1.245873	304.34458	0.014003	
1475.502	20.11891	1.138823	305.902008	0.011746	
1879.58	19.61444	1.19511	307.51832	0.00969	
2299.135	19.99515	0.910048	309.19654	0.007836	
2903.724	19.80644	0.882338	311.614896	0.005614	
3675.125	20.07976	0.470107	314.7005	0.003434	
4424.906	20.15394	0.217673	317.699624	0.001889	
5150.854	20.15331	0.104057	320.603416	0.000825	
5851.01	20.13972	0.05413	323.40404	0.000117	
6523.846	20.12534	0.02823	326.095384	0	
7167.809	20.11333	0.014557	328.671236	0	
7781.478	20.10371	0.007098	331.125912	0	
8364.123	20.09343	0.001647	333.456492	0	
8916.062	20.08292	-0.00203	335.664248	0	
9437.159	20.07114	-0.00449	337.748636	0	
9918.392	20.06209	-0.00541	339.673568	0	
10351.67	20.05387	-0.00558	341.40668	0	
10739.01	20.04557	-0.00525	342.95604	0	
11083.74	20.03736	-0.00455	344.33496	0	
11389.16	20.02689	-0.00329	345.55664	0	
11658.5	20.01003	-0.00089	346.634	0	
11895.04	19.99507	0.001371	347.58016	0	
12131.58	20	0	348.52632	0	

Besides the input_sounding, another input file needed is the input_soil profile. Since the simulation is over a water surface, the deep soil temperature below the surface is not used, but the data is still filled with “soil” temperature of 300K and soil moisture 1.0.

Table 3.2 Values in the input_soil file.

0.0	TSK: 300K	TMN: 300K
Depth (m)	SOILT (K)	SOILM (volumetric fraction)
0.05	300	1.000
0.25	300	1.000
0.7	300	1.000
1.5	300	1.000

WRF does not provide the feature of decreasing skin temperature (TSK), which is the actual surface temperature in the model, with time, which is needed for this study of advection fog moving from warm surface to colder surface. Therefore, the code is modified. Within the file module_first_rk_step_part1.F, which is called at the beginning of each time step, to calculate the tendencies, the following code is added:

```
! Decrease TSK
IF (ANY(grid%tsk.GE.282)) THEN
  grid%tsk = grid%tsk-3*(grid%dt)/3600
ENDIF
```

This piece of code forces the TSK in all grids to decrease by 3 K per hour, until it reaches 282 K. In other words, the model will decrease 3 K per hour for 6 hours from the beginning of the simulation. Since it is called every time step, the dt value is also used for this calculation. This cooling rate is higher than normal. Different cooling rates were test, but given that the SCM is simple and a fog is difficult to form in the model, this cooling rate of 3 K/h is used.

The RRTMG longwave and shortwave radiation schemes (Iacono et al. 2008) use a processor-local random number generator for the cloud coverage so that some of the radiation can penetrate the cloud and some can get scattered. It will not be a problem in the real case simulation where the domain is large and have more clouds. However, from some of the test runs, the result will have significant difference if the schemes are used. Sometimes the programs even gave errors. When the longwave and shortwave schemes are off, the results are identical. Therefore, no radiation is used in the SCM run.

The model uses a time step of 60 s. In our SCM runs there are 101 vertical levels expanding with height, meaning that vertical resolution is higher at low levels than at high level. Although the 37 levels used in the real case simulation are also expanding with height,

they are decided more arbitrarily. In previous experiments, a sensitivity of model results to time step and vertical resolution was observed, so that the results are different with different time steps or vertical resolutions. But such sensitivity is not observed with the current setting. Because the radiation schemes are not used, the solar forcing option is turned off. Various advection features provided in SCM are also turned off. The air column itself is representing a moving air parcel over a cooling water surface via the decreasing surface temperature, so no more advections are needed.

After all settings and inputs were decided, the simulation was run for 4 days starting on Aug. 15. Since there is no radiation and forcing, the date is arbitrary. Data after 24 hours (1600 on Fig. 3.2) will be extracted and analyzed.

3.2 Surface Schemes

In this study, the two surface schemes, Revised MM5 scheme and the MYNN surface scheme are of interest. This chapter will examine the behavior of the two schemes, with YSU and MYNN Level 2.5 PBL schemes. Note that the YSU scheme only accepts the revised MM5 surface scheme while the MYNN Level 2.5 PBL scheme accepts both MM5 and MYNN.

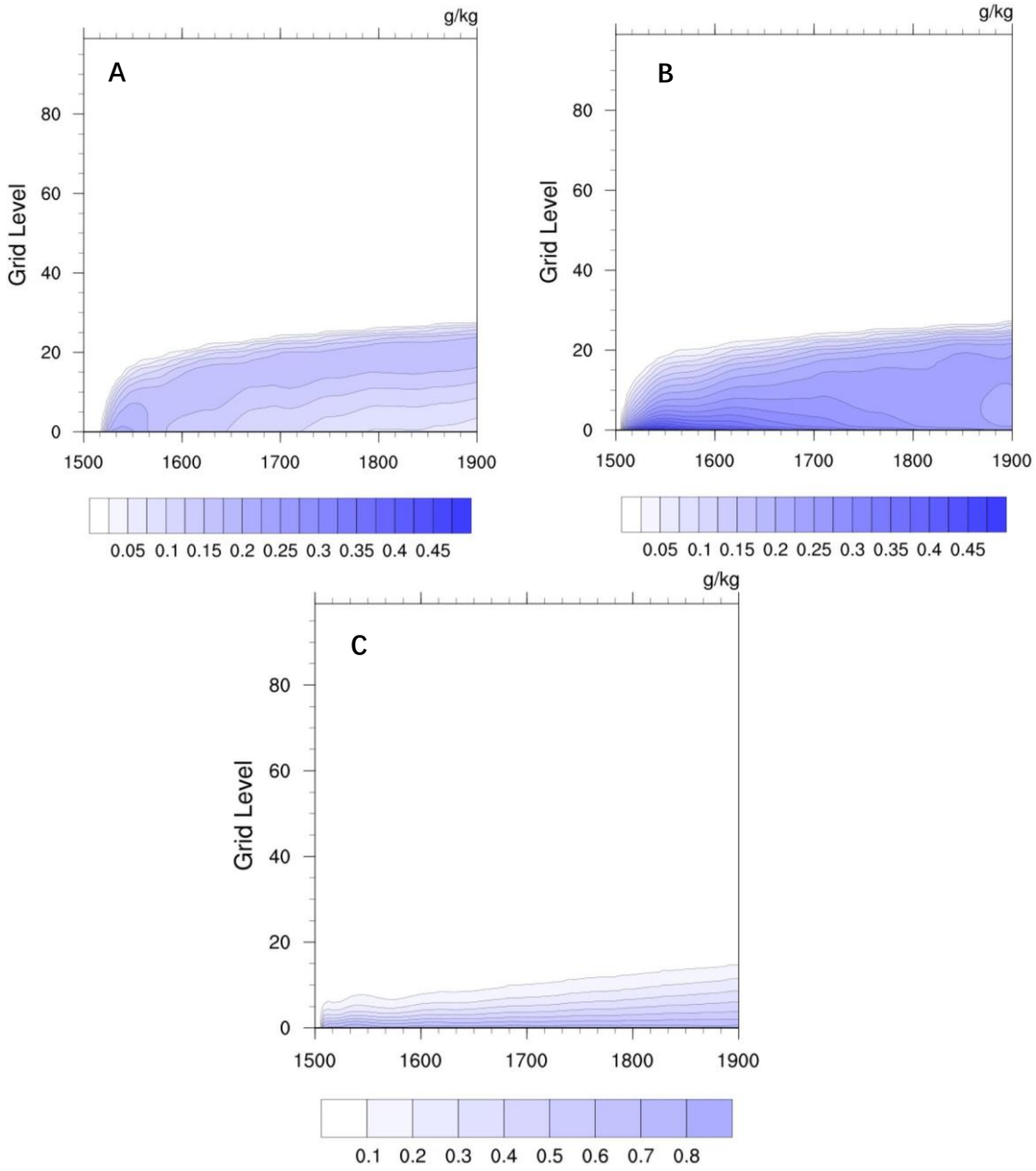

Figure 3.2 QCLOUD contour plots of the simulation period for different settings. Panel A uses MYNN PBL and MYNN surface schemes (MYNN_MYNN below). Panel B uses MYNN PBL and MM5 surface schemes (MYNN_MM5 below). Panel C uses YSU PBL and MM5 surface schemes (YSU_MM5 below). YSU_MM5 gives much more liquid water than the two MYNN cases, so it uses a different colour scale.

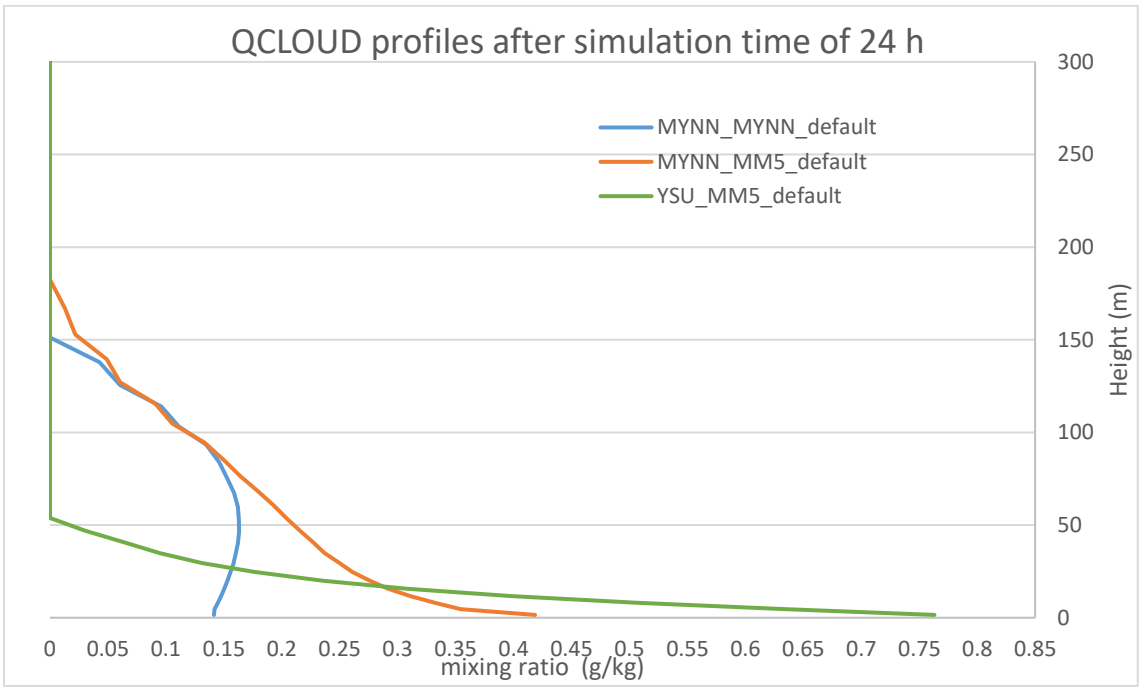
QCLOUD profiles after simulation time of 24 h
MYNN_MYNN_default
MYNN_MM5_default
YSU_MM5_default
300
250
200
150
100
50
0
Height (m)
0
0.05
0.1
0.15
0.2
0.25
0.3
0.35
0.4
0.45
0.5
0.55
0.6
0.65
0.7
0.75
0.8
0.85
mixing ratio (g/kg)

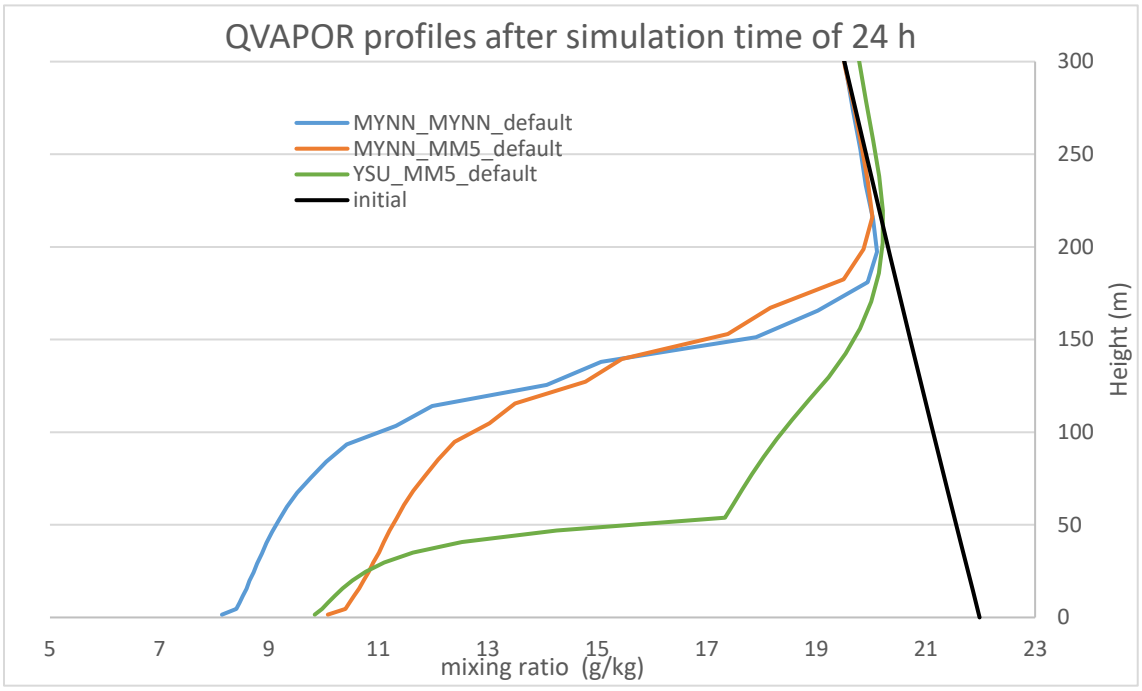
QVAPOR profiles after simulation time of 24 h
MYNN_MYNN_default
MYNN_MM5_default
YSU_MM5_default
initial
300
250
200
150
100
50
0
Height (m)
5
7
9
11
13
15
17
19
21
23
mixing ratio (g/kg)

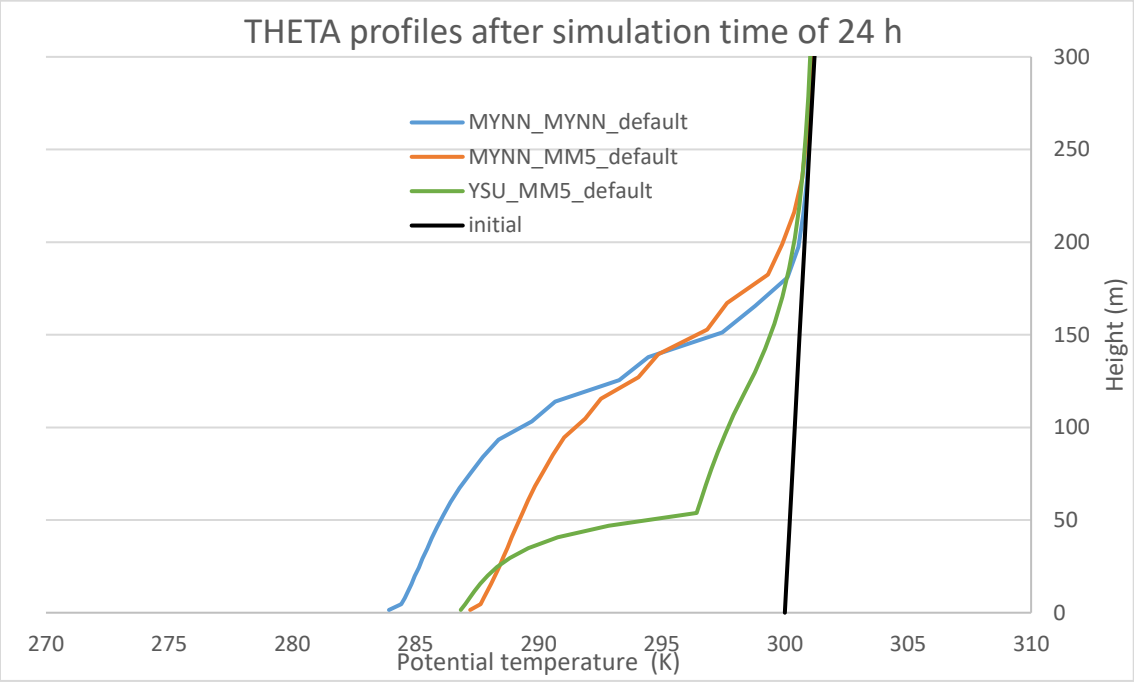

Figure 3.3 QCLOUD, QVAPOR and temperature profiles of the three settings after simulation time of 24 h. The legends indicate the PBL scheme followed by the surface scheme.

Fig. 3.3 shows the profiles of the 3 cases. From the QCLOUD plot, one can see that there is a large difference in the behaviors of the surface schemes near the surface. The case of MYNN_MYNN has a maximum QCLOUD at 50 m, while the other two cases have maximums on the surface and decrease with height, although MYNN_MYNN and MYNN_MM5 are using the same PBL scheme. Therefore, the QCLOUD behavior near surface may be dominated by the surface scheme. The MYNN surface scheme has a maximum aloft while the MM5 scheme treats the surface as a source of QCLOUD with much higher value than the MYNN surface scheme, especially using with YSU PBL scheme. In

section 1.2.2, it is mentioned that some observations from Kunkel (1984) and Pinnick et al (1978) show that QCLOUD increases with height in near surface levels. Therefore, the MYNN surface scheme seems to catch the behavior correctly, and it gives much lower condensation than the MM5 surface scheme. Above 50 m, MYNN_MYNN and MYNN_MM5 have close values while YSU_MM5 has no more liquid water. It shows that the MYNN PBL scheme has a thicker fog of 150 m than the YSU PBL scheme giving a denser but lower fog, and the PBL scheme will dominate the behavior in the atmosphere.

From the QVAPOR plot, one can see that the YSU PBL scheme has a lot of water vapor in 50-150 m. Although the two MYNN PBL cases also predict maxima in that height range, the amount is much lower, which suggests that the QVAPOR profile in the atmosphere is also dominated by the PBL scheme. The YSU PBL scheme is a nonlocal scheme, so it is able to represent deeper convection in the air column than the MYNN PBL scheme which is a local scheme. The vertical grids in the MYNN PBL scheme can only respond to the adjacent grids in each time step, so the changes in the meteorological variables may be slower. Also, YSU_MM5 has more liquid water and water vapor under 200 m. The water can only come from the surface in this single column model without advection, suggesting that the YSU PBL scheme will get more water from the water surface.

From the THETA plot, it can still be found that the two settings with the MM5 scheme are close at the surface, but MYNN_MM5 gets closer to MYNN_MYNN in the aloft. The YSU_MM5 setting has a sharp change at 50 m for both QVAPOR and THETA, which is the fog top of this setting.

3.3 Gravitational Settling

WRF provides a feature of gravitational settling of fog/cloud droplets, which can be turned on by using grav_settling = 1 or 2 in the namelist. Grav_settling = 1 uses the Duynkerke (1991) method in the atmosphere and at the surface. When grav_settling is set to be 2, the Katata et al. (2008) method will be used at the surface and Duynkerke (1991) will be used only in the atmosphere.

Duynkerke (1991) uses a simple formula for deposition velocity:

$$v_d = gno * QC^{2/3} \tag{3.1}$$

where QC is the QCLOUD value from WRF and gno is a constant. Duynkerke uses gno = 4.64 originally, but a comment in the code says that the value is considered to be too aggressive and gno = 1 is used in the program instead.

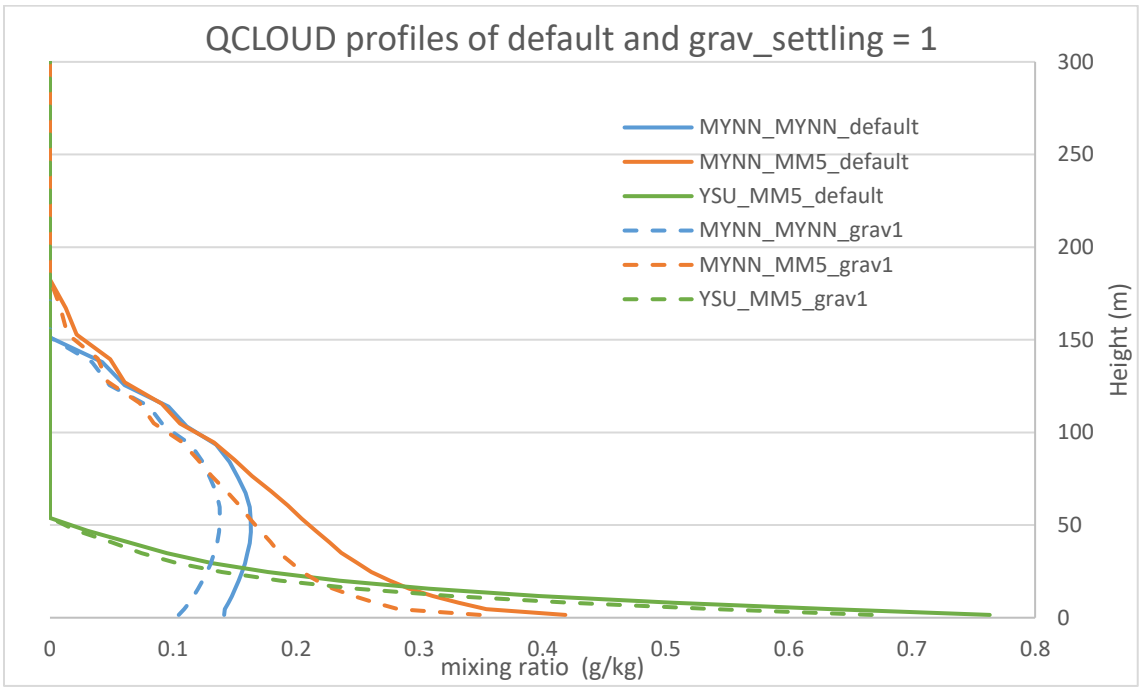
QCLOUD profiles of default and grav_settling = 1
MYNN_MYNN_default
MYNN_MM5_default
YSU_MM5_default
MYNN_MYNN_grav1
MYNN_MM5_grav1
YSU_MM5_grav1
Height (m)
0
50
100
150
200
250
300
0
0.1
0.2
0.3
0.4
0.5
0.6
0.7
0.8
mixing ratio (g/kg)

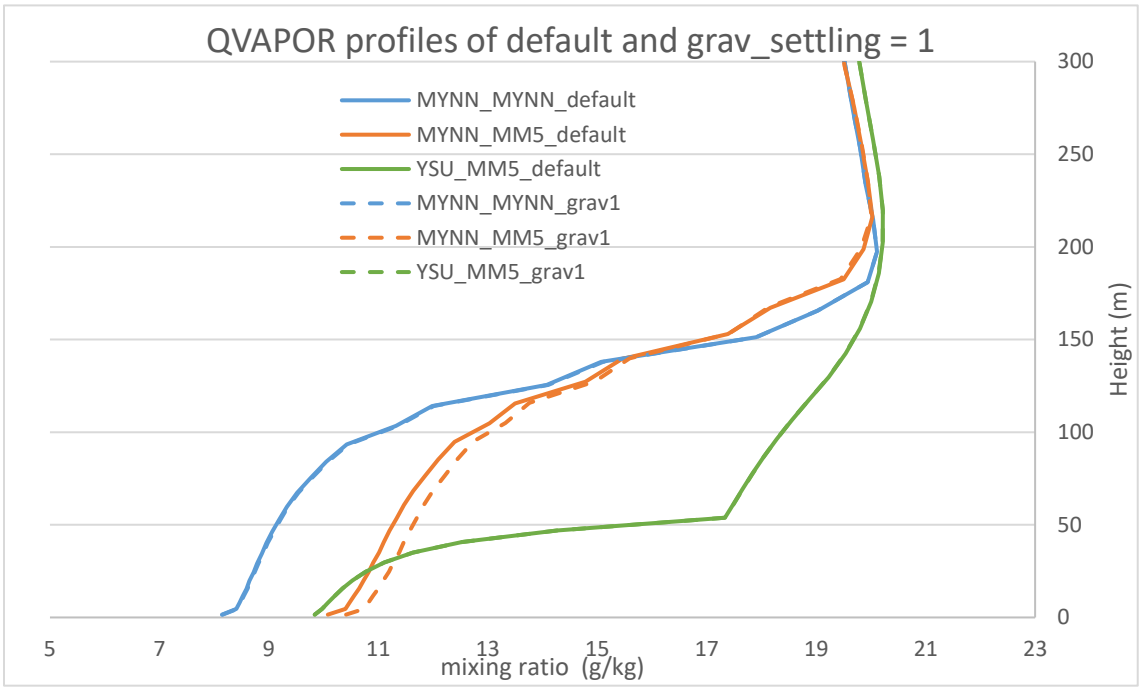
QVAPOR profiles of default and grav_settling = 1
MYNN_MYNN_default
MYNN_MM5_default
YSU_MM5_default
MYNN_MYNN_grav1
MYNN_MM5_grav1
YSU_MM5_grav1
Height (m)
0
50
100
150
200
250
300
5
7
9
11
13
15
17
19
21
23
mixing ratio (g/kg)

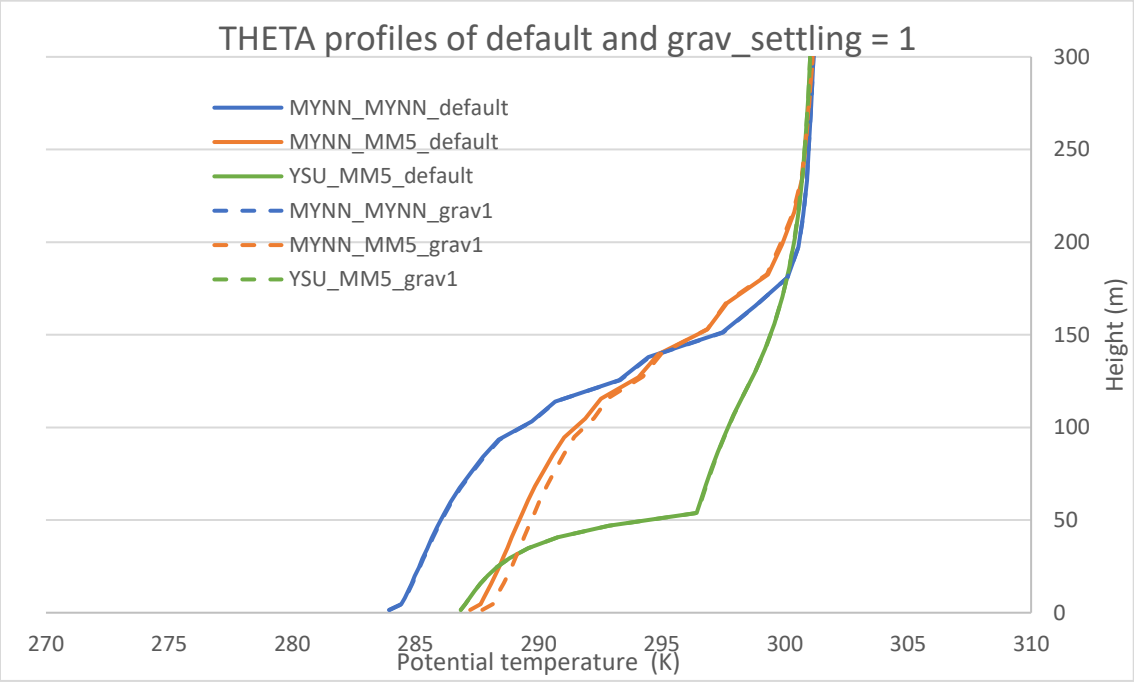

Figure 3.4 QCLOUD, QVAPOR and THETA plots of the three settings, with default WRF and grav_settling = 1.

Fig. 3.4 shows how grav_settling = 1 works. QVAPOR and THETA are not affected in MYNN_MYNN and YSU_MM5. But MYNN_MM5 has slight differences under 150 m. It removes some liquid water, depending on the amount of liquid water at the level. However, from 1.2.2 again, near surface the liquid water should increases with height. The deposition should depend on height; lower levels should decrease a larger fraction of liquid water than higher levels. The Duynkerke (1991) method is not ideal for our goal to match the observations.

Katata et al. (2008) studied fog deposition in the forest and proposed a simple linear

function for a fog deposition velocity on land. For different vegetation categories, different constants are used according to their research results. For the category "others", including water surface, the following equation is used:

$$v_s = \frac{g d_p^2 (\rho_w - \rho)}{18\mu} \tag{3.2}$$

where $d_p = (17.03 * LWC * 10^3 + 9.72) * 10^{-6}$ in m is the mean fog droplet diameter, g is gravitational acceleration, ρ_w is water density, ρ is air density and μ is viscosity of air. This is simply a gravitational settling velocity. The empirical approach of the droplet diameter can be a problem. Kunkel (1980) showed that the correlation between mean terminal speed and LWC was poor.

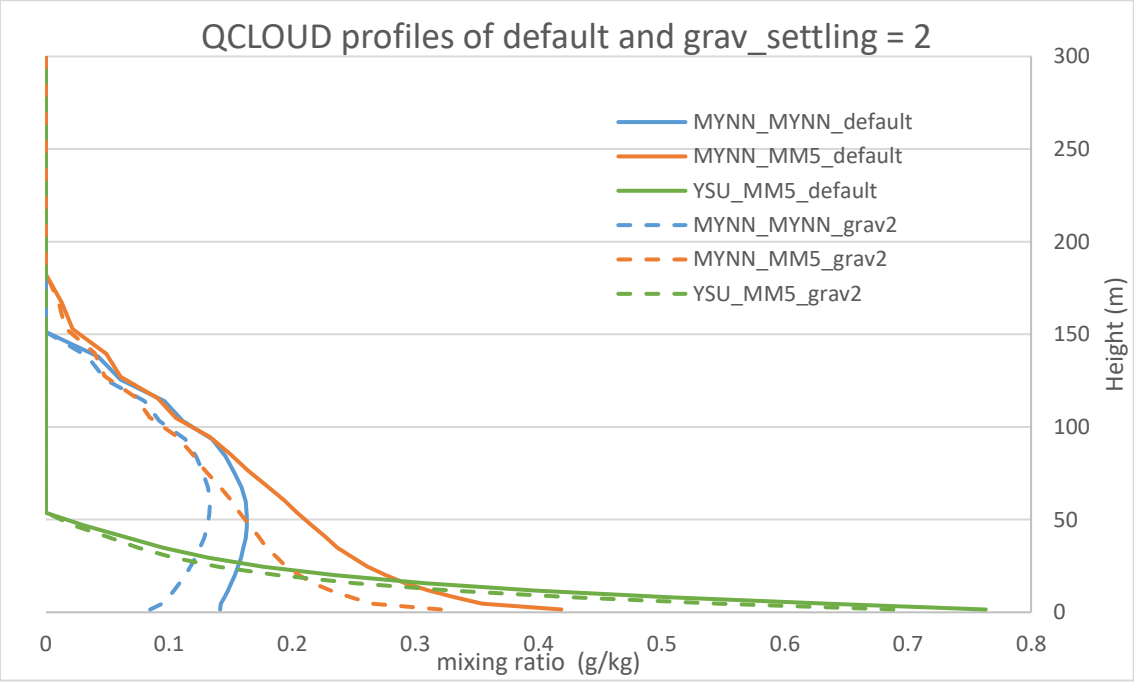

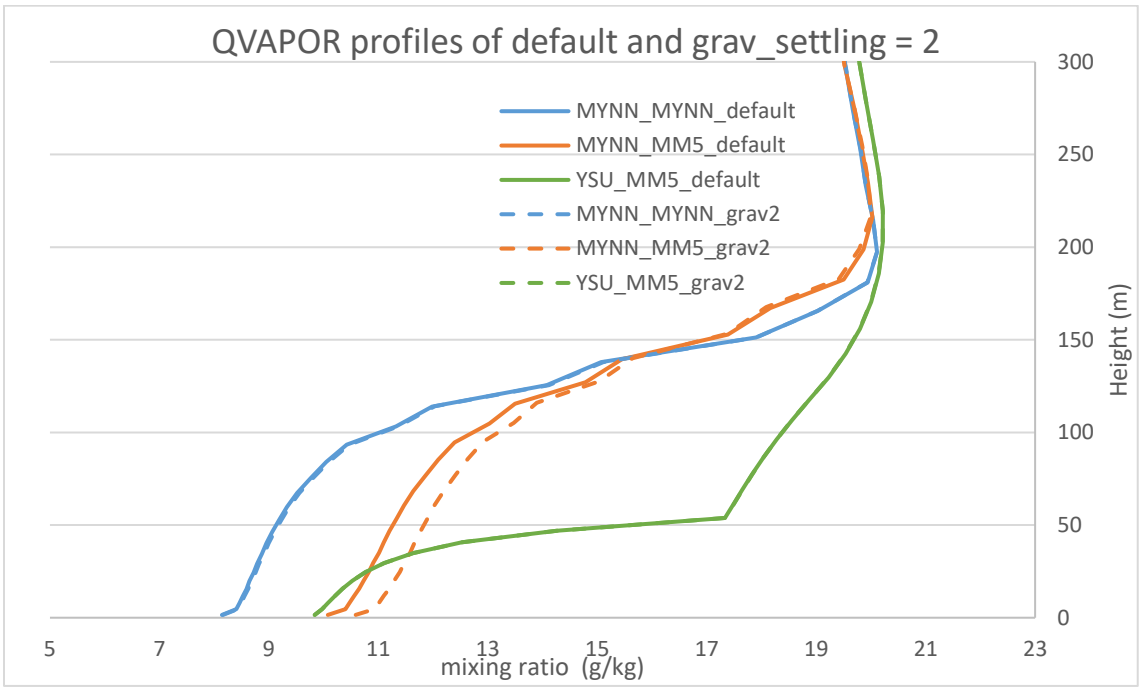

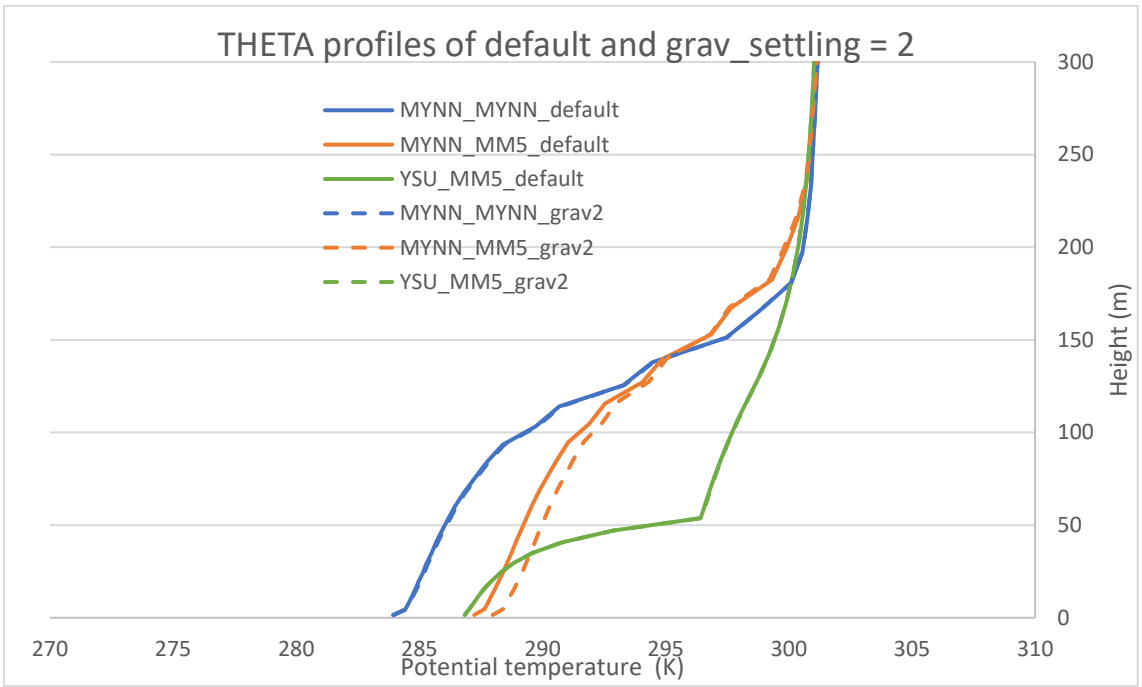

Figure 3.5 QCLOUD, QVAPOR and THETA plots of the three settings, with default WRF and grav_settling = 2.

Grav_settling = 2 is similar to option 1. It removes more liquid water at the surface using the Katata et al. (2008) method and keeps the Duynkerke (1991) method aloft. Only the first grid level has some changes from grav_settling = 1, but not significant, so it does not match the observations too. Another problem is that the Katata et al. (2008) method is not specific for a water surface. Water surface is in the "OTHER" category, along with urban land, mixed forest, and snow etc.

According to the MYNN manual (Olson et al. 2019), previously the grav_settling feature could only be used with MYNN PBL scheme, but it works for any PBL scheme now. It also mentions that the Thompson microphysics scheme has its own droplet deposition, therefore, users should avoid using both grav_settling and the Thompson microphysics scheme in the simulation, which is the case in the test of grav_settling = 1 and 2. But there is no warning in any WRF documentations, and it is unknown if it is safe to use both now, although the related code of gravitational deposition is found in the Thompson microphysics scheme. It has no deposition to the surface, but deals with flux differences associated with settling velocity. It can be turned off by setting av_c = 0 in the code. All the results above do not modify the code of Thompson microphysics, but only Fig. 3.6 below is a comparison of av_c = 0 and the default setting.

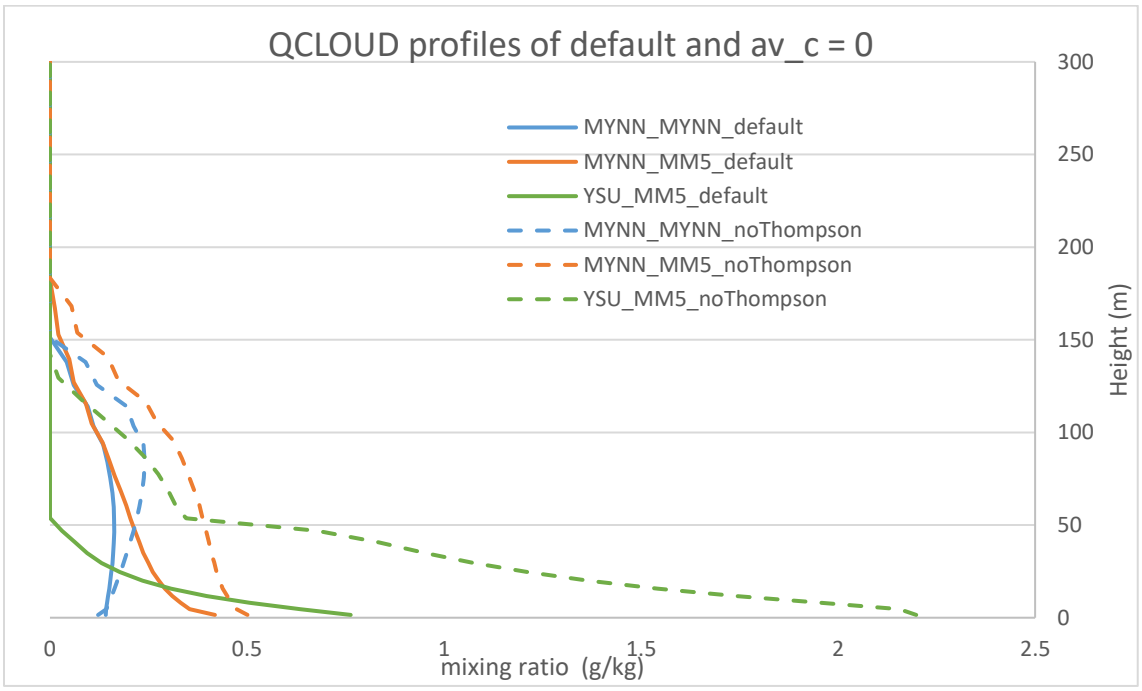
QCLOUD profiles of default and av_c = 0
MYNN_MYNN_default
MYNN_MM5_default
YSU_MM5_default
MYNN_MYNN_noThompson
MYNN_MM5_noThompson
YSU_MM5_noThompson
300
250
200
150
100
50
0
Height (m)
0
0.5
1
1.5
2
2.5
mixing ratio (g/kg)

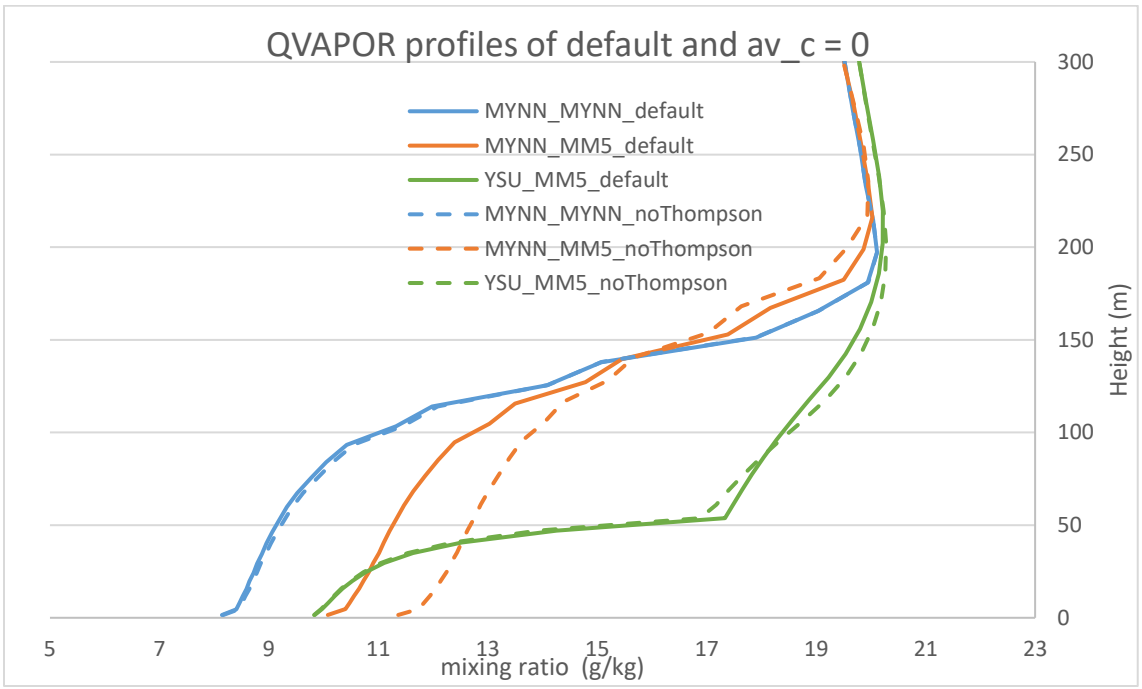
QVAPOR profiles of default and av_c = 0
MYNN_MYNN_default
MYNN_MM5_default
YSU_MM5_default
MYNN_MYNN_noThompson
MYNN_MM5_noThompson
YSU_MM5_noThompson
300
250
200
150
100
50
0
Height (m)
5
7
9
11
13
15
17
19
21
23
mixing ratio (g/kg)

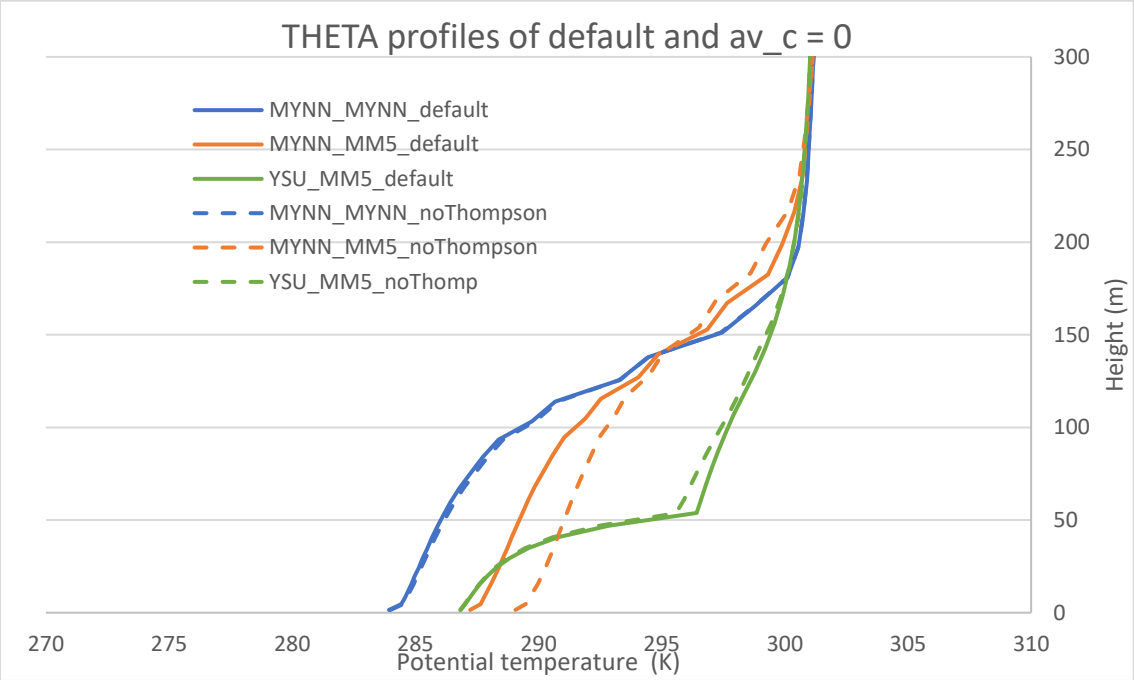

Figure 3.6 QCLOUD, QVAPOR and THETA plots of the three settings, with default WRF and av_c = 0 in the Thompson microphysics.

Thompson microphysics has removed a lot of liquid water for the YSU_MM5 case, not only the amount but also the thickness. It is also significant in the two MYNN cases. This comparison has more changes to QVAPOR and THETA than the two grav_settling comparisons where the lines of MYNN_MYNN and YSU_MM5 simply overlap. The difference in MYNN_MM5 is also larger. It suggests that the deposition velocity in the Thompson microphysics is important to water vapor and heat, not simply a removal of liquid water. Also, the code of the Thompson microphysics scheme is difficult to understand, without enough descriptions and comments. We consider that the Thompson microphysics scheme needs more study, and the modification of the code is not easy or straightforward.

So, this research will keep the default Thompson microphysics code and use its gravitational settling rather than the grav_settling feature in the namelist.

3.4 Turbulent Deposition

We have proposed a method to decrease the amount of liquid water in WRF, where deposition to the surface by turbulent mixing is introduced. From Isaac and Hallett (2005), fog droplets are likely to coalesce with the ocean surface, then the droplets should be removed, leading to QC = 0 at the surface, and QC can have a log profile in the constant flux layer near the surface. In this layer, some fog droplets are deposited to the surface by turbulent mixing, which is dependent on height. Such turbulent deposition is represented via a deposition velocity written as

$$v_d = \frac{u^* k}{\ln\left(\frac{z1 + z0_c}{z0_c}\right)} \tag{3.3}$$

where u* is friction velocity, k is von Karman constant, z1 is height of the lowest model level and z0c is a new parameter, a roughness length for fog droplets. Roughness lengths are used to represent different processes for turbulent transfers of heat, water vapor and momentum to the surface, and they need not all be the same. Therefore, the value of z0c is unknown, and requires field research. To apply this method to WRF program, the code in the two PBL schemes is modified.

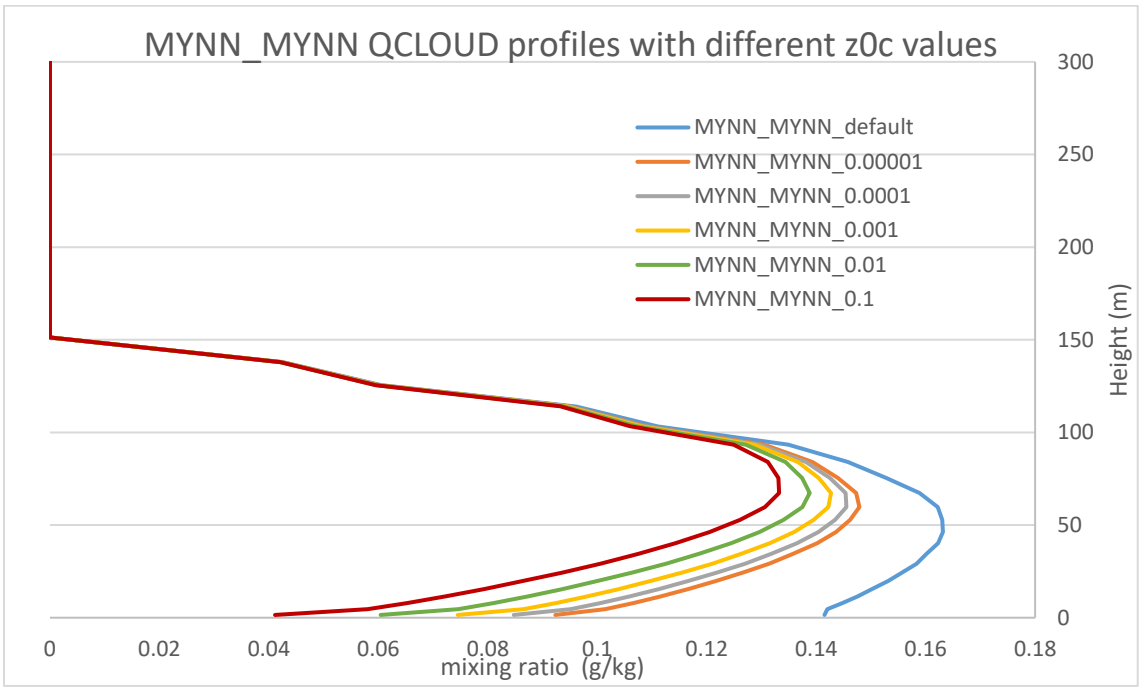
MYNN_MYNN QCLOUD profiles with different z0c values
MYNN_MYNN_default
MYNN_MYNN_0.00001
MYNN_MYNN_0.0001
MYNN_MYNN_0.001
MYNN_MYNN_0.01
MYNN_MYNN_0.1
Height (m)
300
250
200
150
100
50
0
0
0.02
0.04
0.06
0.08
0.1
0.12
0.14
0.16
0.18
mixing ratio (g/kg)

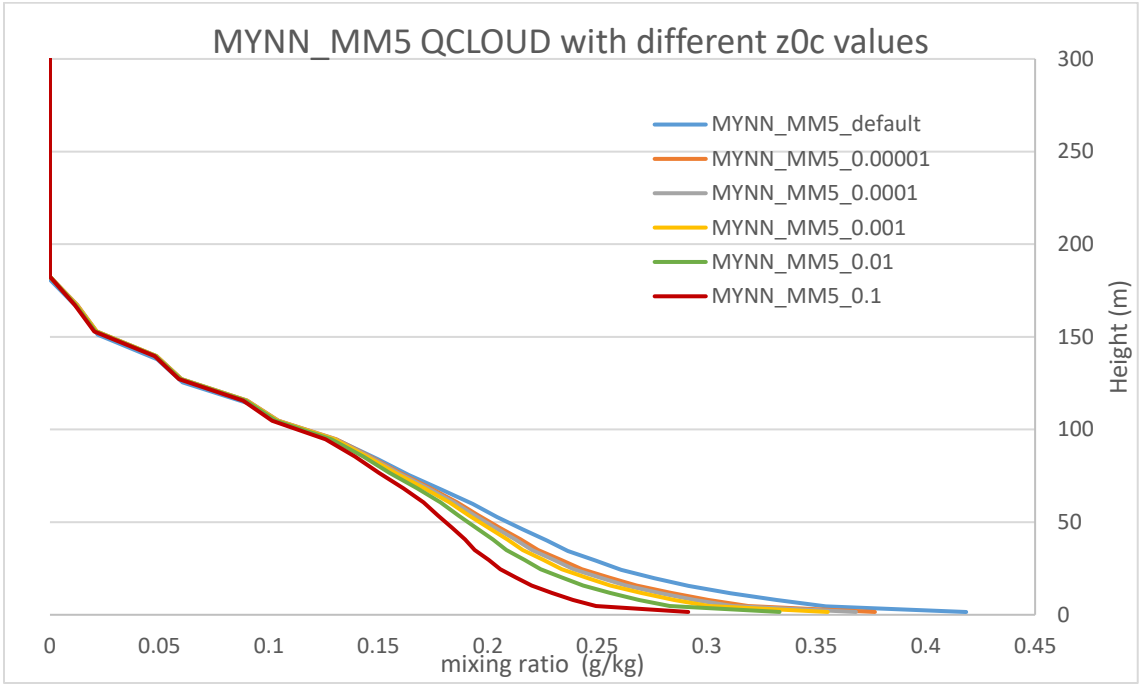
MYNN_MM5 QCLOUD with different z0c values
MYNN_MM5_default
MYNN_MM5_0.00001
MYNN_MM5_0.0001
MYNN_MM5_0.001
MYNN_MM5_0.01
MYNN_MM5_0.1
Height (m)
300
250
200
150
100
50
0
0
0.05
0.1
0.15
0.2
0.25
0.3
0.35
0.4
0.45
mixing ratio (g/kg)

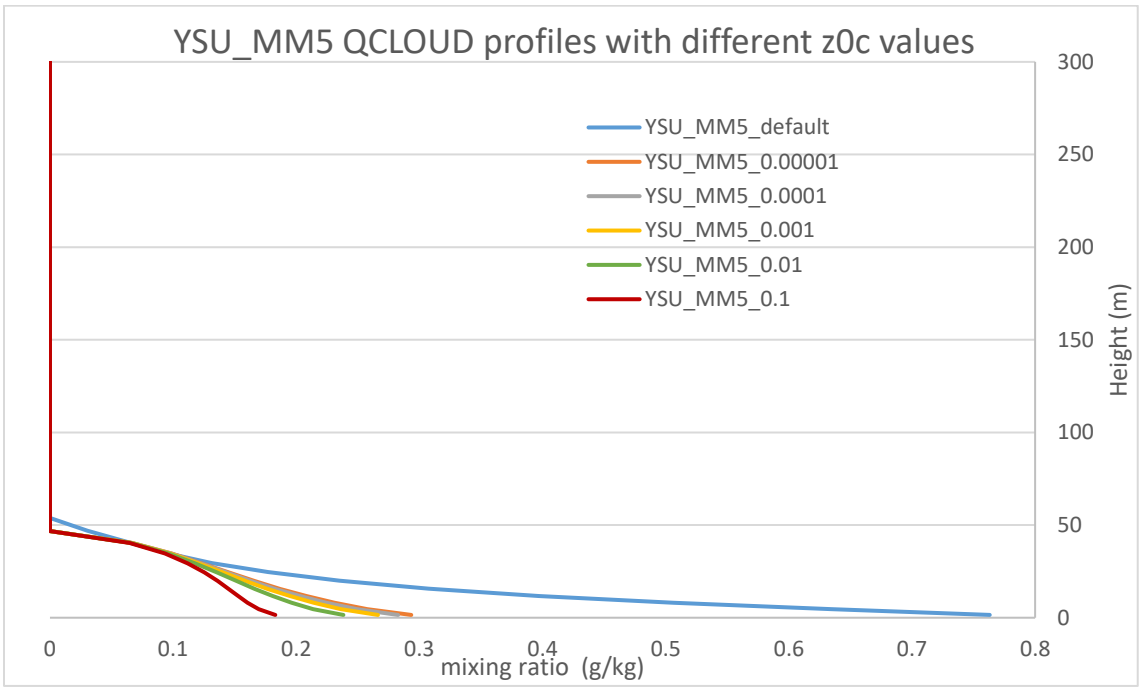
YSU_MM5 QCLOUD profiles with different z0c values
YSU_MM5_default
YSU_MM5_0.00001
YSU_MM5_0.0001
YSU_MM5_0.001
YSU_MM5_0.01
YSU_MM5_0.1
300
250
200
150
100
50
0
Height (m)
0
0.1
0.2
0.3
0.4
0.5
0.6
0.7
0.8
mixing ratio (g/kg)

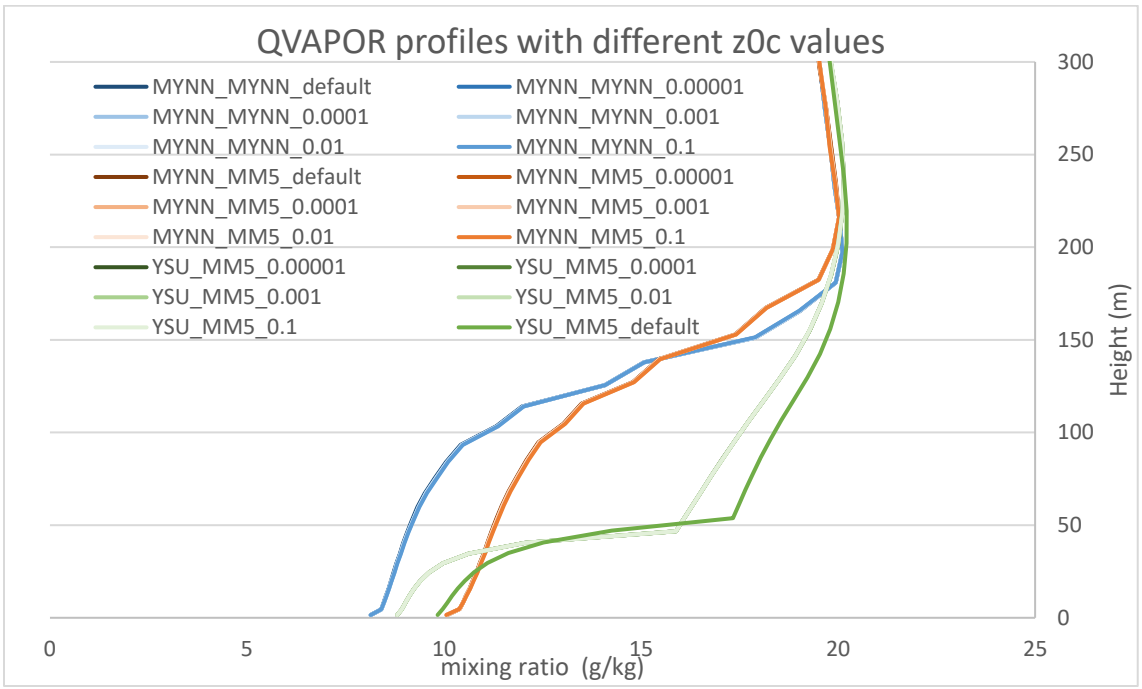
QVAPOR profiles with different z0c values
MYNN_MYNN_default
MYNN_MYNN_0.00001
MYNN_MYNN_0.0001
MYNN_MYNN_0.001
MYNN_MYNN_0.01
MYNN_MYNN_0.1
MYNN_MM5_default
MYNN_MM5_0.00001
MYNN_MM5_0.0001
MYNN_MM5_0.001
MYNN_MM5_0.01
MYNN_MM5_0.1
YSU_MM5_0.00001
YSU_MM5_0.0001
YSU_MM5_0.001
YSU_MM5_0.01
YSU_MM5_0.1
YSU_MM5_default
300
250
200
150
100
50
0
Height (m)
0
5
10
15
20
25
mixing ratio (g/kg)

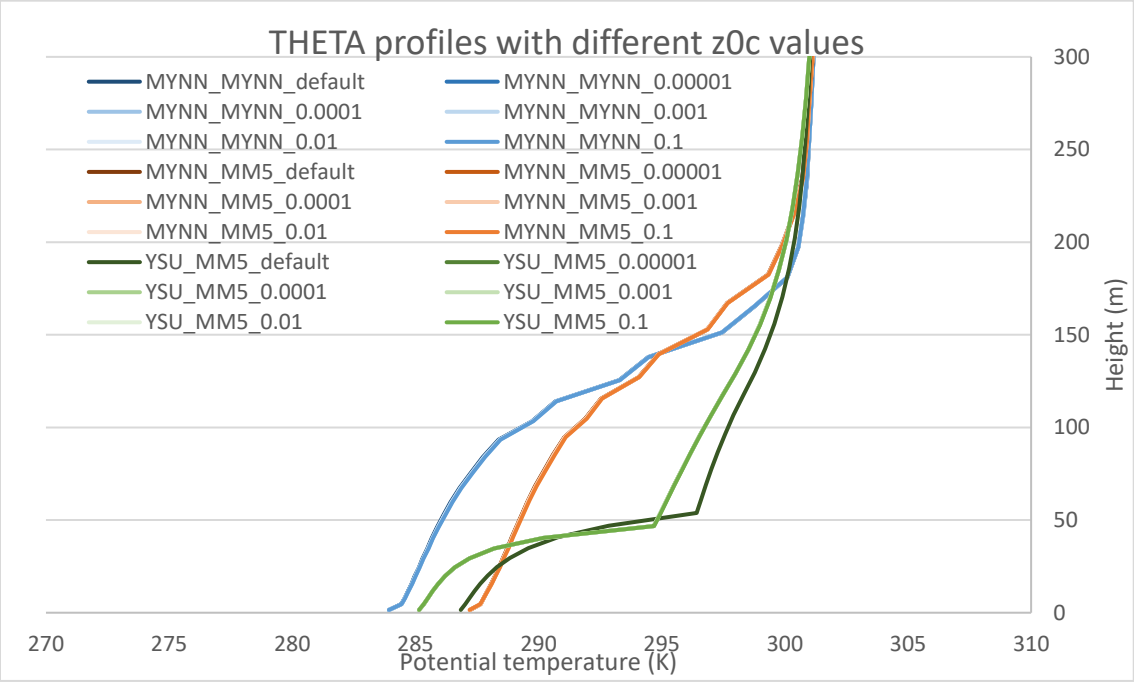

Figure 3.7 QCLOUD, QVAPOR and THETA plots of the three settings, with z0c from 0.00001 to 0.1. Most lines overlap in the QVAPOR and THETA plot, showing that different z0c values have no impact on water vapor and temperature.

Fig. 3.7 shows the behavior of the modification. Turbulent deposition has most impact under 100m. For all the three settings, larger z0c values will remove more liquid water, and the removal is decreasing with height. As one can expect, such modification will give a fog layer with increasing QCLOUD near surface, matching the observation. Since the two MM5 settings have their maxima at the surface, a much larger z0c value is needed to reach our expectation. The reason why MM5 surface scheme has such behavior needs further study.

Different z0c does not affect the values of QVAPOR and THETA in all settings. The YSU_MM5 is affected when the modification is applied. This may come from the different

mechanisms of the two PBL schemes, or the modification in the YSU PBL scheme can be improved.

3.5 Discussion

In this chapter, the single column model within WRF is used to simulate an advection fog. The code in WRF is edited, to give a cooling with time at the surface, and to allow a provided vertical level profile. A sounding with decreasing relative humidity with height, and stable profile is used as an input to the model's initial condition. Three settings are of interest, MYNN_MYNN, MYNN_MM5, and YSU_MM5. They all have different behaviors. MYNN_MYNN has maximum amount of liquid water in the middle of the fog, while the other two have their maxima at the surface, due to the difference of the surface schemes. YSU_MM5 gives much more liquid water, and has a lower fog top than the others, showing the difference of the PBL schemes. Different methods of gravitational settling of fog droplets within WRF are tested in all the three settings. Duynkerke (1991) and Katata et al. (2008) methods can be turned on by grav_settling in the namelist. They give similar results, and they do not help to reach the observation. The Thompson microphysics scheme also has a gravitational settling, which removes a significant amount of liquid water. According to the MYNN manual, using both Thompson microphysics scheme and grav_settling option will cause a double counting problem, so only the Thompson microphysics method is kept for gravitational settling. Turbulent deposition maybe the key to the problem. In the constant flux layer near surface, the profile of cloud water can be considered as linearly decreasing in

a log scale as other variables like vapor or heat. By applying a log relationship, the liquid water can be removed depending on the height, with lower levels removing more liquid water than higher levels, which will give a desired profile of QCLOUD. However, the roughness length for fog droplets, z0c, used in the equation, is unknown and needs further study. It cannot be concluded from the SCM test, since the model is too simple and shouldn't be compared to the observation. After the study of SCM, it is found that MYNN_MYNN is the best setting for now, since the MM5 surface scheme gives too much liquid water at the surface. In the next chapter, MYNN PBL scheme with MYNN surface scheme, modified with turbulent deposition will be applied to the real case simulation to see its improvement.

Chapter 4

Real Case Simulation Re-examined

In this chapter, the real case simulation in WRF has been used again to simulate fog in summer 2018. Domains are the same as Chapter 2, the physics parameterization is the same as Table 2.1. This parameterization has MYNN PBL and MYNN surface schemes, the setting that seems to work the best from Chapter 3. One difference from Chapter 2 is that this time the MYNN PBL scheme is modified with turbulent deposition, to see the improvement of the modification in real case simulation. In addition, because the modification works under 100 m, it is assumed that the model requires a higher vertical resolution in lower levels to represent turbulent transfers near the surface. Therefore, the two sets of vertical levels, 37 levels used in the real case study in Chapter 2 and 101 levels used in the SCM study in Chapter 3 are used for comparison.

4.1 Experiment

4.1.1 Experiment Set Up

As discussed in Chapter 3, the z0c value in the modification is unknown. Therefore, in this experiment, simulations have been done over a 3-day period, August 14 12Z to 17 12Z 2018, the same period as experiment 1 in Chapter 2, with five different z0c values, from 0.00001 to 0.1. Horizontal grid resolutions are 30 km and 10 km in the nested grids (1 and 2 in Fig. 2.1) as before. Only gravitational settling from the Thompson microphysics scheme is used, grav_settling is 0.

4.1.2 Results

From Fig. 4.1, The time series of visibility at the first model level of the real case simulation is not satisfactory. In either 37 levels or 101 levels, the default WRF follows the same trend as the modified runs. In general, different runs with 101 levels have larger difference than with 37 levels, with 16 00Z to 12Z being an example. However, the 101-level simulations give a miss before 16 00Z.

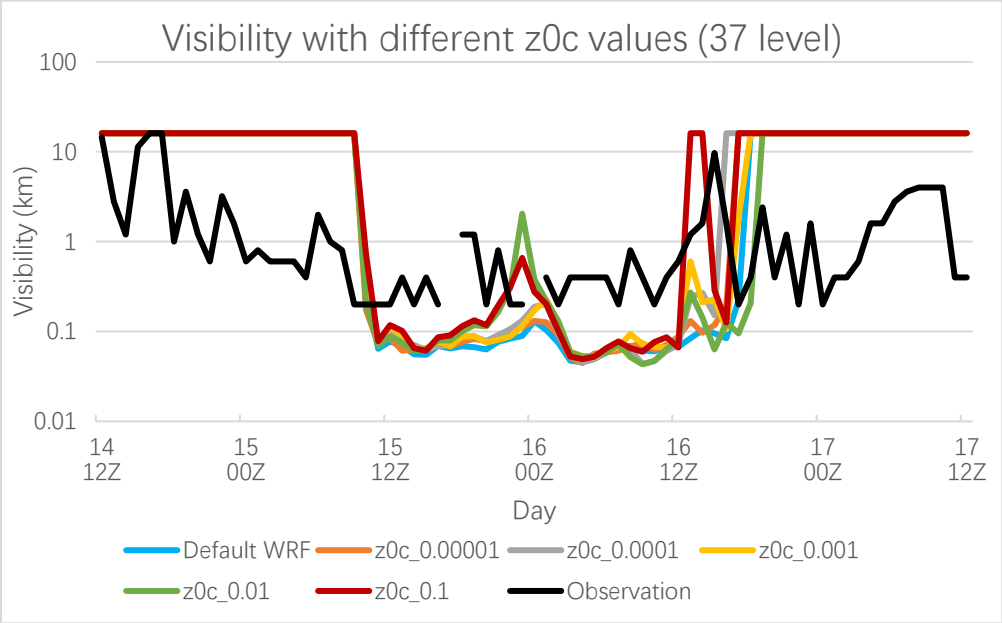

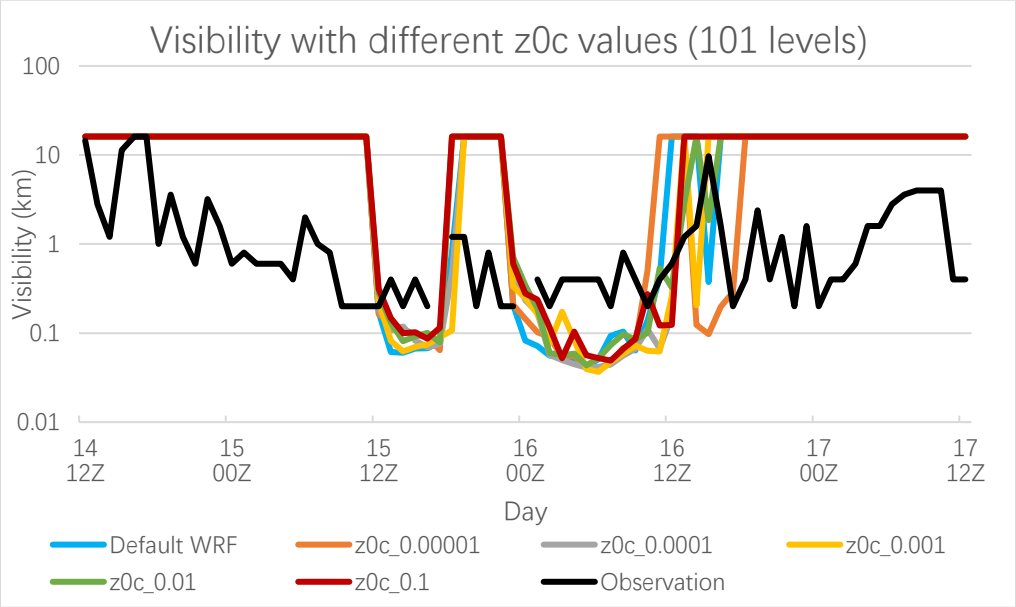

Figure 4.1 Time series of visibility calculated with the Isaac et al. (2020) formula, including the observation, the default (not-modified) WRF, and modified WRF with 5 different z0c values, and with 2 vertical level settings. Results are at the first grid level, which is near 17 m for 37 levels and 2 m for 101 levels. The observation is at 2 m. Two data points of 0 km visibility, at 15 17Z and 16 00Z in observation cannot be shown in a logarithmic scale.

Table 4.1 QCLOUD values ($g\ kg^{-1}$) at Aug 16th, 00Z of the different runs with 37 vertical levels at the first 4 model levels. Top row includes z0c values (m) used. The output from the NCL script has 7 decimal places.

Height (m)	default	z0c_0.00001	z0c_0.0001	z0c_0.001	z0c_0.01	z0c_0.1
16.43425	0.213918	0.077823	0.045198	0.052064	0.01565	0.025431
45.31314	0.142504	0.046139	0.001768	0	0.010294	0.006212
78.83207	0.036982	0.012652	0	0	0	0
121.1585	0	0.001883	0	0	0	0

Since only a few grid levels contain QCLOUD, it is better to show the numbers for each model level in Table 4.1 rather than a vertical profile plot. The z0c modification removes more than half of the liquid water compared to the default run at this time step, but as in Fig. 4.1, it is not the case in the whole period. Also, a higher z0c value does not necessarily give less liquid water.

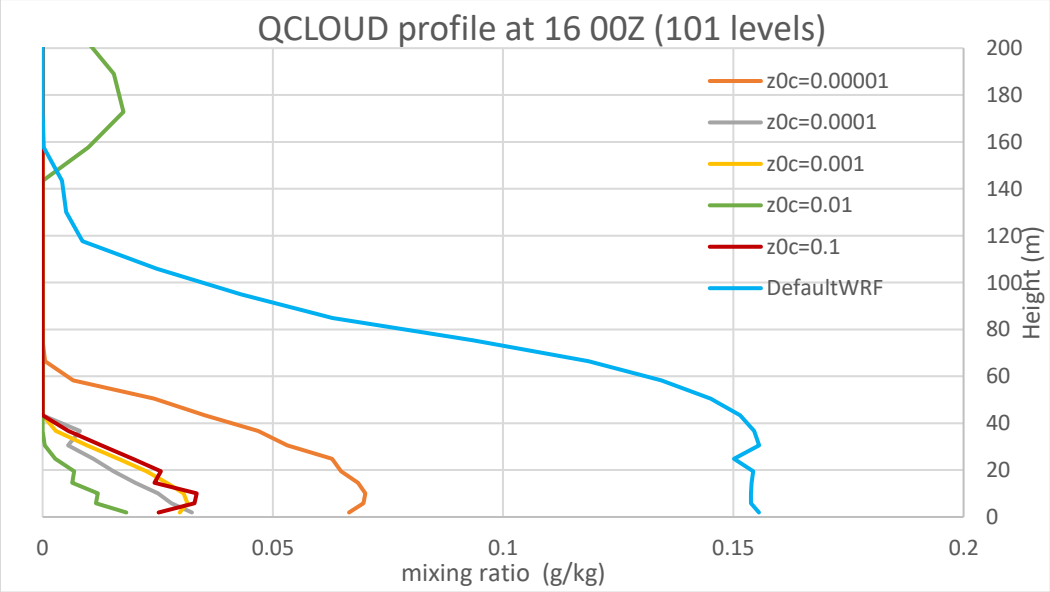

Figure 4.2 QCLOUD profiles at Aug. 16th, 00Z from the different runs with 101 levels. z0c values are in m.

When 101 levels are used, the modification seems to work better. It decreases liquid water mixing ratio considerably compared to the default WRF. The computation with z0c = 0.00001 m has the highest QCLOUD values relative to other modified runs in all levels up to 80 m. However, z0c = 0.01 m is the one with lowest QCLOUD, rather than z0c = 0.1 m, and it also has some low cloud from 140 m, which shows that these near surface modifications can also affect liquid water concentrations aloft. Note that z0c = 0.1, 0.001, 0.0001 m are very close so results may not be too sensitive to the precise value used.

4.2 Discussion

In this chapter, we applied the z0c modification of adding turbulent deposition to the real case simulation. Since compared to the ideal case study, the real case simulation is much more complicated, including radiation and advection, it is not expected to have as clear results as in the single column model results shown in Chapter 3.

The results show that the z0c modification does not always decrease the liquid water. In some periods it may have more liquid water than the default run, and higher z0c value does not always give less liquid water than lower z0c values. In the real case simulation, the liquid water can come from advection, and radiation can interact with the droplets. Two different vertical level settings are used, 37 levels used in Chapter 2 and 101 levels used in Chapter 3. It is found that with 101 levels, the differences between different simulations are larger than with only 37 levels, showing that with higher vertical resolutions near surface,

different conditions can be better represented. However, simulations with 101 level give a miss in fog. Since the liquid water would not disappear, it is suggested that vertical resolution can have impact on the horizonal distribution.

When the modification successfully decreases the liquid water, the visibility is still not high enough to reach the observation. The droplet number can be a problem. It is treated as a constant of 10^8 m^{-3} in the formula, but certainly it should be a variable. The gravitational settling and turbulent deposition should decrease the droplet number as well as the mixing ratio, and the number can also vary by other factors, including sea spray from breaking waves. Some microphysics schemes, e.g. the aerosol-aware Thompson scheme (Thompson et al 2014) (mp_physics = 28) follow the number of aerosol particles. However, the number is not available in WRF output by default, so it requires the modification to the WRF program, and at the moment the turbulent deposition simply decreases the liquid water according to the height, not involving the droplet number, which requires further work. The droplet size can also be a problem. Although it is not in the formula of Isaac et al. (2020), different sizes can affect the visibility differently. The Thompson microphysics scheme uses a generalized gamma distribution for droplet size,

$$N(D) = \frac{N_t}{\Gamma(\mu + 1)} \lambda^{\mu+1} D^{\mu} e^{-\lambda D} \tag{4.1}$$

where N_t is the total number of particles in the distribution, D is the particle diameter, λ is the distribution's slope and μ is the shape parameter. For cloud water over ocean, as mentioned above, N=10^8 m^{-3}, and μ=12. In the scheme, D is calculated from different processes like condensation and collision. This distribution may not be true near surface.

Chapter 5

Conclusion

In this study, the WRF model version 4.1.2 has been used in an attempt to examine the accuracy of marine fog forecasting. Although fog can seriously affect transportation and public safety, the lack of observations and parameterization uncertainties make fog forecasting difficult. The interest location considered is Sable Island (44˚N, 60˚W), with more than 200 hours of fog in June and July per year on the island. The long and narrow shape of the island makes it an ideal location to study marine weather. Model results have been compared to the hourly reports from the ECCC station on the island.

In Chapter 2, in the real case simulation (em_real), different physics options in WRF are tested to have a good parameterization as the starting point for the study. The parameterization in Table 2.2 is selected. The results of the daily 36 h simulations over summer 2018 show that the model gives a much lower visibility at the first vertical level compared to the observations. Two visibility algorithms used in the calculation both use liquid water concentration. Therefore, it is considered that there is too much liquid water being predicted when fog appears in the model. In addition, 2 m temperature, 10 m wind

speed and direction, and 2 m water vapor mixing ratio are compared. None of them seems to be responsible for the overpredicted amount of liquid water.

In Chapter 3, the single column model of the idealized case simulations in WRF (em_scm_xy) is used. The temperature at the model surface is set to be decreasing with time to simulate the movement of an advection fog over colder water surface. An input sounding, designed to have higher relative humidity near surface, is used in the model for fog formation. Three physics settings, MYNN_MYNN, MYNN_MM5, YSU_MM5, as named by the PBL scheme followed by the surface scheme are tested. The MYNN_MYNN setting, with the maximum QCLOUD in the middle of the fog, seems to catch the behavior from the observation correctly. The other two settings with MM5 surface scheme, predict QCLOUD maxima at the surface. The gravitation settling options in WRF are examined. Both option 1 and 2 give very similar results, and they do not help to get us closer to the observation with QCLOUD increasing with height near surface. The turbulent deposition has been added to the model by modifying the code and tested. The results show that the QCLOUD can be lowered according to the height.

In Chapter 4, the turbulent deposition modification is tested in the real case simulation. The results show that the z0c modification does not always decrease the amount of liquid water, because the real case simulation is more complicated. It has advection and radiation, which are not included in the SCM study. In some periods when the modification works well, the model visibility is still too low, indicating that other factors such as droplet number or droplet size may play a role in the visibility, and they should be considered in the calculation

of visibility.

There are many options for future study. The MM5 surface scheme, which gives the maximum of QCLOUD at the surface, does not match the observation. Therefore, a modification to that scheme is of interest. A trade off between resolution and run time is important for operational use. A higher vertical resolution is done in Chapter 4 and higher horizontal resolution study is done in Appendix A. A higher resolution run may decrease the number of false alarms, but it takes a longer time to finish. Lastly, field studies are necessary for the improvement of fog forecasting. A correct value of z0c is needed for the modification of turbulent deposition. Droplet numbers and droplet size are also of interest in the field study.

Bibliography

Bonekamp, P. N. J., Collier, E., & Immerzeel W.W., 2018: The Impact of Spatial Resolution, Land Use, and Spinup Time on Resolving Spatial Precipitation Patterns in the Himalayas. *Journal of Hydrometeorology*, **19**(10), 1565-1581. https://doi.org/10.1175/JHM-D-17-0212.1

Chen, C., Zhang, M., Perrie, W., Chang, R., Chen, X., Duplessis, P., and Wheeler, M., 2020: Boundary Layer Parameterizations to Simulate Fog Over Atlantic Canada Waters. *Earth and Space Science*, **7**(3), e2019EA000703. https://doi.org/10.1029/2019EA000703

Cohen, A. E., Cavallo, S. M., Coniglio, M. C., and Brooks, H. E., 2015: A Review of Planetary Boundary Layer Parameterization Schemes and Their Sensitivity in Simulating Southeastern U.S. Cold Season Severe Weather Environments. *Weather and Forecasting*, **30**(3), 591-612. https://doi.org/10.1175/WAF-D-14-00105.1

de La Fuente, Y., Delage, Y., Desjardines, S., MacAfee, A., Pearson, G., and Ritchie, H., 2007: Can Sea Fog be Inferred from Operational GEM Forecast Fields? *Pure appl. geophys.*, **164**, 1303-1325. https://doi.org/10.1007/s00024-007-0220-9

Duynkerke, P. G., 1991: Radiation Fog: A Comparison of Model Simulation with Detailed Observations. *Monthly Weather Review*, **119**(2), 324-341. https://doi.org/10.1175/1520-0493(1991)119%3C0324:RFACOM%3E2.0.CO;2

Findlanter, J., Roach, W., and McHugh, B. 1989: The haar of north-east Scotland. *Quarterly Journal of the Royal Meteorological Society*, **115**(487). 581-608. https://doi.org/10.1002/qj.49711548709

Gultepe I, Muller, M.D., and Boybeyi, Z. 2006: A new visibility parametrization for warm fog applications in numerical weather prediction models. *J. Appl. Meteorol.* **45**, 1469–1480. https://doi.org/10.1175/JAM2423.1

Hong, S., Noh, Y., and Dudhia, J., 2006: A New Vertical Diffusion Package with an Explicit Treatment of Entrainment Processes. *Monthly Weather Review*, **134**(9), 2318-2341. https://doi.org/10.1175/MWR3199.1

Iacono, M. J., Delamere, J. S., Mlawer, E, J., Shephard, M. W., Clough, S. A., and Collins, W. D., 2008: Radiative forcing by long-lived greenhouse gases: Calculations with the AER radiative transfer models. *Journal of Geophysical Research*, **113**, D13103. https://doi.org/10.1029/2008JD009944

Isaac, G. A., Bullock, T., Beale, J., and Beale, S., 2020: Characterizing and Predicting Marine Fog Offshore Newfoundland and Labrador. *Weather and Forecasting*, **35**(2), 347-365. https://doi.org/10.1175/WAF-D-19-0085.1

Isaac, G. A. and Hallett, J., 2005: Clouds and Precipitation. In M. G. Anderson (Eds.), *Encyclopedia of Hydrological Science*. https://doi.org/10.1002/0470848944.hsa031

Jiménez, P. A., Dudhia, J., González-Rouco, J. F., Navarro, J., Montávez, J. P., and García-Bustamante, E., 2012: A Revised Scheme for the WRF Surface Layer Formulation. *Monthly Weather Review*, **140**(3), 898-918. https://doi.org/10.1175/MWR-D-11-00056.1

Katata, G., Nagai, H., Wrzesinsky, T., Klemm, O., Eugster, W., and Burkard, R., 2008: Development of a Land Surface Model Including Cloud Water Deposition on Vegetation. *Journal of Applied Meteorology and Climatology*, **47**(8), 2129-2146. https://doi.org/10.1175/2008JAMC1758.1

Kunkel, A., 1984: Parameterization of droplet terminal velocity and extinction coefficient in fog models. *J. Climate Appl. Meteor.*, **23**, 34-41.

Lin, C., Zhang, Z., Pu, Z., and Wang, F., 2017: Numerical simulations of an advection fog event over Shanghai Pudong International Airport with the WRF model. *Journal of Meteorological Research*, **31**, 874-889. https://doi.org/10.1007/s13351-017-6187-2

Monthith, J., Unsworth, M., 2007. *Principles of Environmental Physics.* Third Ed. Academic Press

Nakanishi, M., and Niino, H., 2006: An Improved Mellor–Yamada Level-3 Model: Its Numerical Stability and Application to a Regional Prediction of Advection Fog. *Boundary-Layer Meteorology*. **119**, 397-407. https://doi.org/10.1007/s10546-005-9030-8

Nakanishi, M., and Niino, H., 2009: Development of an Improved Turbulence Closure Model for the Atmospheric Boundary Layer. *Journal of the Meteorological Society of Japan*, **87**, 895-912. https://doi.org/10.2151/jmsj.87.895

National Centers for Environmental Prediction/National Weather Service/NOAA/U.S. Department of Commerce. 2015, updated daily. NCEP GDAS/FNL 0.25 Degree Global Tropospheric Analyses and Forecast Grids. Research Data Archive at the National Center for Atmospheric Research, Computational and Information Systems Laboratory. https://doi.org/10.5065/D65Q4T4Z. Accessed - 20 Feb 2021.

Olson, J. B., Kenyon, J. S., Angevine, W. A., Brown, J. M., Pagowski, M., and Suselj, K., 2019: A Description of the MYNN-EDMF Scheme and the Coupling to Other Components in WRF–ARW. NOAA Technical Memorandum OAR GSD-61. https://doi.org/10.25923/n9wm-be49

Pinnick, R. G., Hoihjelle, D. L., Fernandez, G., Stenmark, E. B., Lindberg, J. D., Hoidale, G. B., and Jennings, S. G., 1978: Vertical structure in atmospheric fog and haze and its effect on visible and infrared extinction. *J. Atmos. Sci.*, **35**, 2020–2032.

Riordan, D. and Hansen, B. K., 2002: A fuzzy case-based system for weather prediction. *Eng. Int. Syst.*, **3**, 139–146.

Skamarock, W. C., Klemp, J. B., Dudhia, J., Gill, D. O., Liu, Z., Berner, J., Wei Wang, J. G. Powers, M.G. Duda, D., M. Barker and Huang, X., 2019: A Description of the Advanced Research WRF Model Version 4 (No. 771 NCAR/TN-556+STR). http://dx.doi.org/10.5065/1dfh-6p97

Taylor, G. I., 1917: The formation of fog and mist. *Quarterly Journal of the Royal Meteorological Society*, **43**(183), 241-268. https://doi.org/10.1002/qj.49704318302

Taylor, P. A., Salmon, J. R. & Stewart, R.E., 1993: Mesoscale observations of surface fronts and low pressure centres in Canadian East Coast winter storms. *Boundary-Layer Meteorology*, 64, 15–54. https://doi.org/10.1007/BF00705661

The NCAR Command Language (Version 6.6.2) [Software]. (2019). Boulder, Colorado: UCAR/NCAR/CISL/TDD. http://dx.doi.org/10.5065/D6WD3XH5

Thompson, G., and Eidhammer, T., 2014: A Study of Aerosol Impacts on Clouds and Precipitation Development in a Large Winter Cyclone. *Journal of the Atmospheric Sciences*, **71**(10), 3636-3658. https://doi.org/10.1175/JAS-D-13-0305.1

Thompson., G., Field, P. R., Rasmussen, R. M., and Hall, W. D., 2008: Explicit Forecasts of Winter Precipitation Using an Improved Bulk Microphysics Scheme. Part II: Implementation of a New Snow Parameterization. *Monthly Weather Review*, **136**(12), 5095-5115. https://doi.org/10.1175/2008MWR2387.1

Wilkinson, J. M., Porson, A. N. F., Bornemann, F. J., Weeks, M., Field, P. R., and Lock, A. P. 2013: Improved microphysical parametrization of drizzle and fog for operational forecasting using the Met Office Unified Model. *Quarterly Journal of the Royal Meteorological Society*, **139**, 488–500. https://doi.org/10.1002/qj.1975

Wilson, T. H., and Fovell, R. G., 2017: Modeling the Evolution and Life Cycle of Radiative Cold Pools and Fog. *Weather and Forecasting*, **33**(1), 203-220.

https://doi.org/10.1175/WAF-D-17-0109.1

Yang, L., Liu, J.-W., Ren, Z.-P., Xie, S.-P., Zhang, S.-P., and Gao, S.-H., 2018: Atmospheric conditions for advection- radiation fog over the western Yellow Sea. *Journal of Geophysical Research: Atmospheres*, **123**(10), 5455–5468. https://doi.org/10.1029/2017JD028088

Zhang, S. P., and Ren, Z. P., 2010: The influence of thermal effects of underlaying surface on the spring sea fog over the Yellow Sea – Observations and numerical simulation (in Chinese). *Acta Meteological Sinica*, **68**, 116-125.

Appendix A

Higher Horizontal Resolution

In Chapter 2, the model 2 m temperature is found to be relatively constant without any diurnal cycle, due to the water surface at the grid point. In this chapter, a higher horizontal resolution has been used to see the effect of the land surface on visibility.

A.1 Observation

A diurnal cycle can be seen from Fig. A1. On average, 2 m temperature at the Sable Island ECCC measurement station increases after 11 a.m UTC, 7 am AST. Also August was hotter than July, and July was hotter than June.

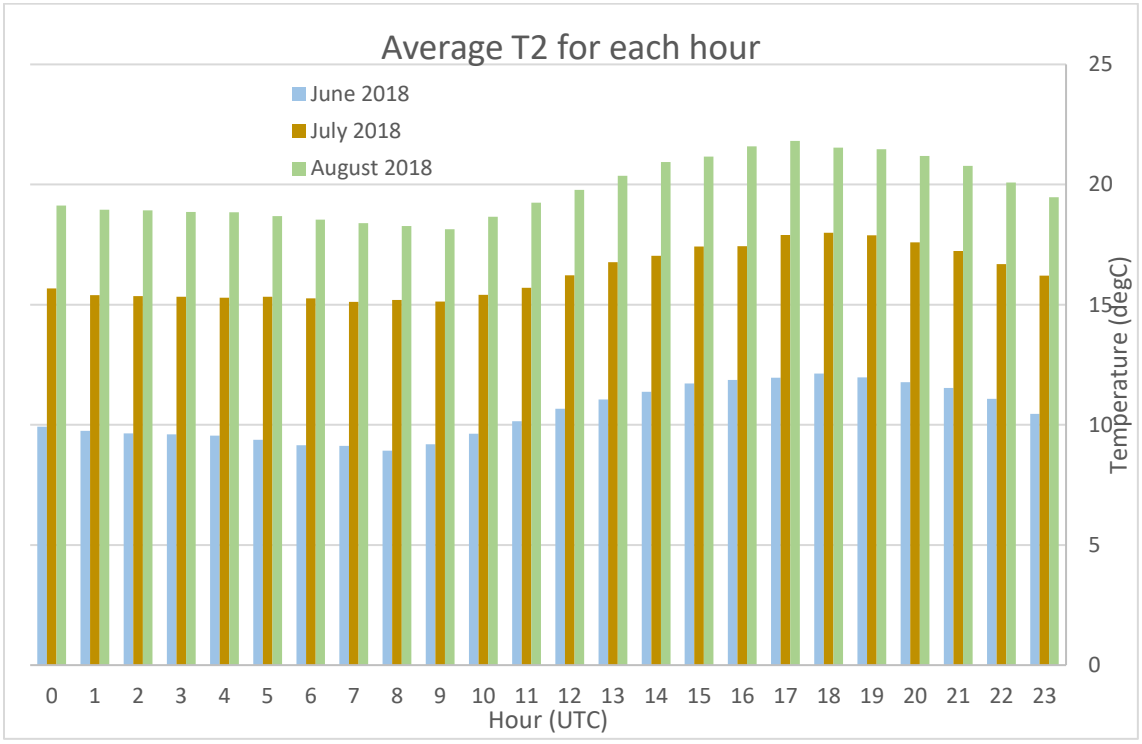

Figure A1 Monthly averaged observed 2 m temperature on Sable Island at indicated UTC hours of the day. Data for June, July and August 2018 are separated.

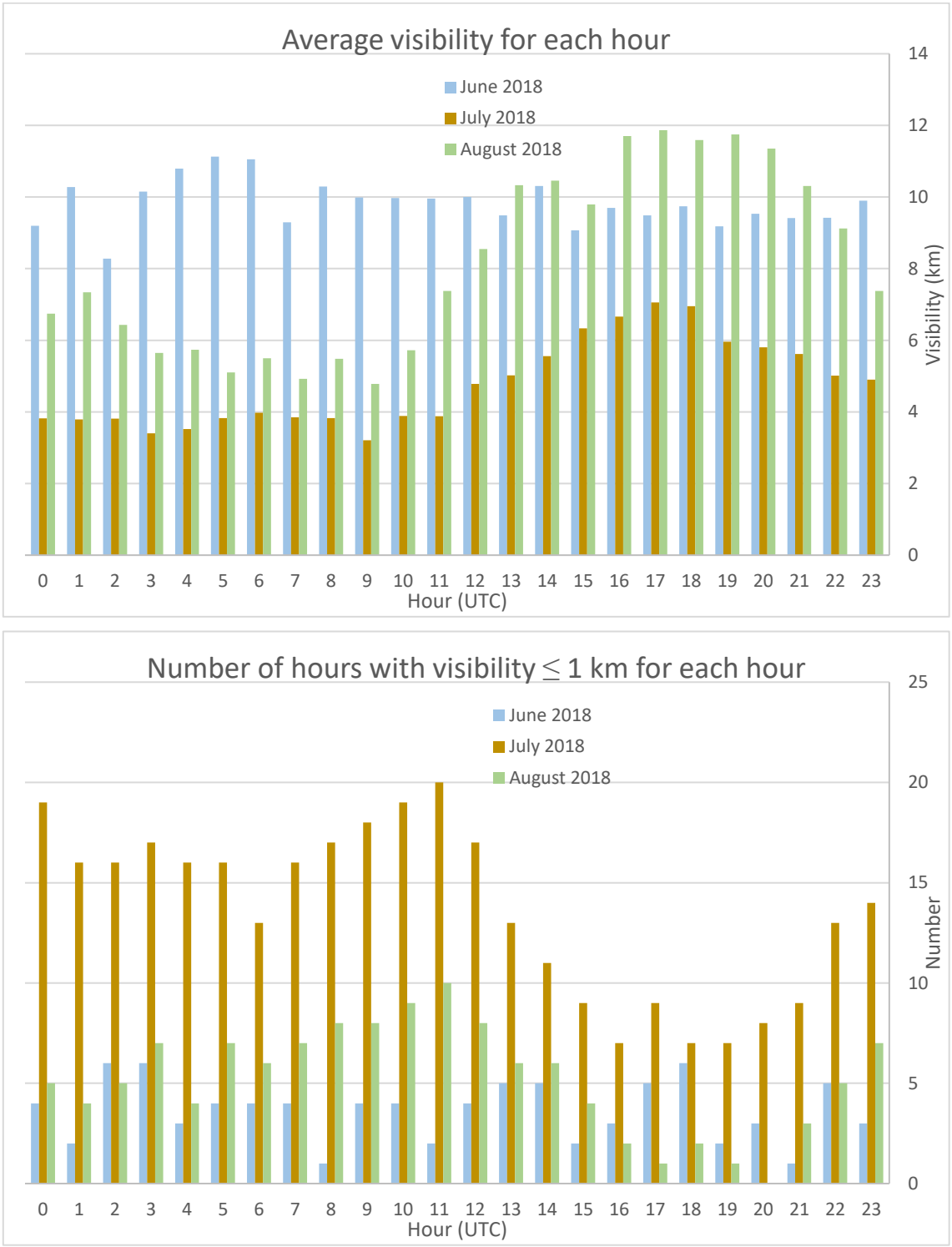

Figure A2 Hourly visibility and number with visibility ≤ 1 km for each hours. Monyhly averaged data in June, July and August 2018 are separated.

Because June had the least number of fogs in the three months, its average visibility was always relatively high, not showing a diurnal cycle. July had the most numbers of fog, and a diurnal cycle can be seen from both the average visibility and the number of hours. The same trend can also be seen in August. After 11 a.m. UTC, when the temperature starts to increase, fogs will dissipate and visibility will increase.

A.2 Experiment Set Up

Two additional domains (both have 181 x 181 points), with higher horizontal resolution dx=2 km and dx=400 m, are set around Sable Island (Fig. A3 Top). The land area of the Sable Island can be seen in this resolution (Fig. A3 bottom). The grid point (i=107, j=57) in the middle of the island is selected for result comparisons.

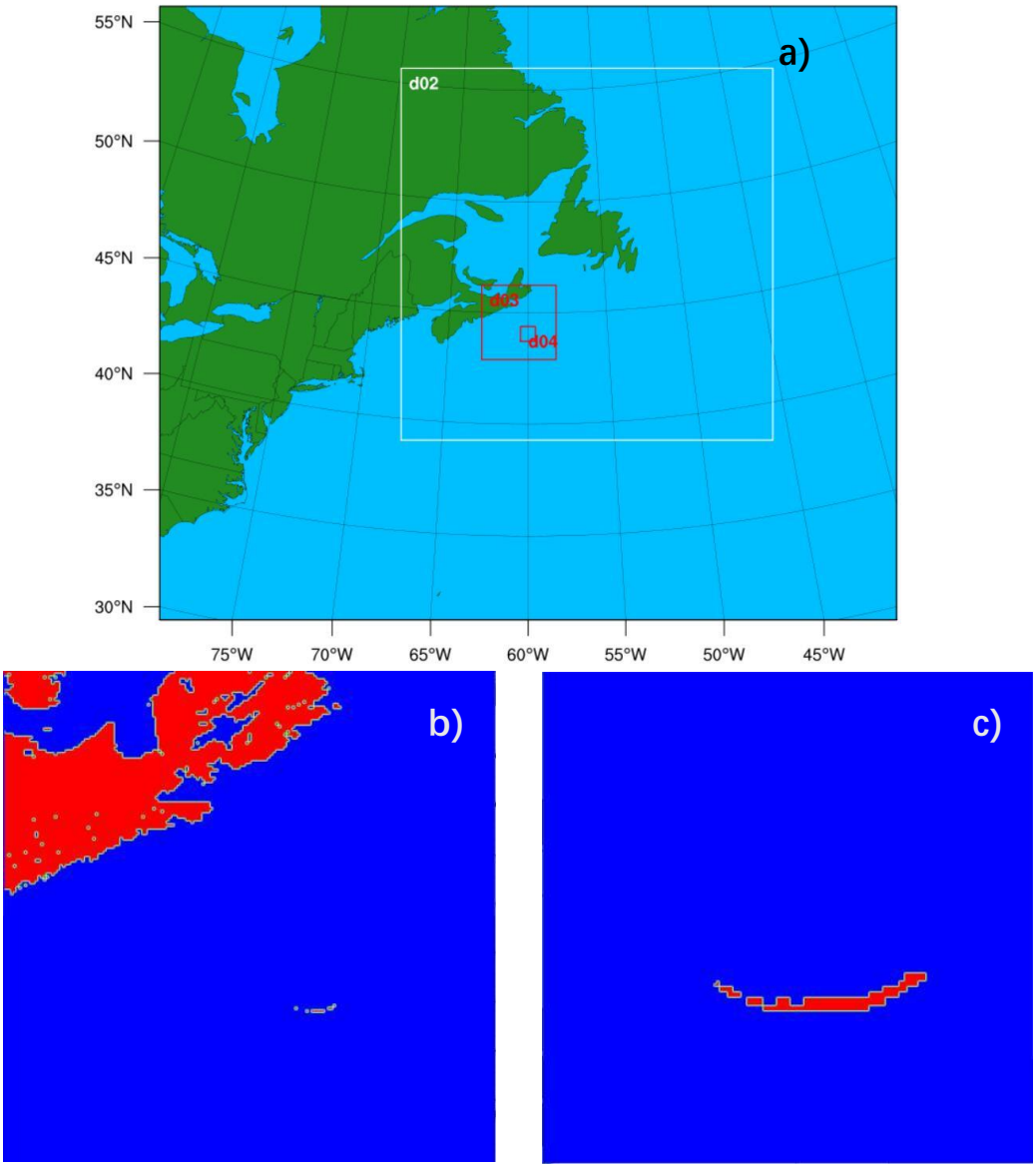

Figure A3 (a): The overview of the four domains used in this experiment. (b): Landmask in domain 3. The land of Sable Island can be seen in this resolution. (c): Landmask in domain 4. The land covers more grid points.

This experiment keeps same the parameters in Table 2.1, and does the same 36 hours

simulations as in Chapter 2. Considering that a simulation at this resolution requires much more computation cost and time (It needs more than 4 hours to finsh one daily simulation of 36 hours, while the two-domains run only needs 40 minutes.), this experiment only covers July 1 00Z to July 7 00Z, where there were 60 hours with visibility ≤ 1 km in a total of 145 hours. The default WRF and modified WRF with z0c = 0.1 m have been used.

A.3 Result

Temperature

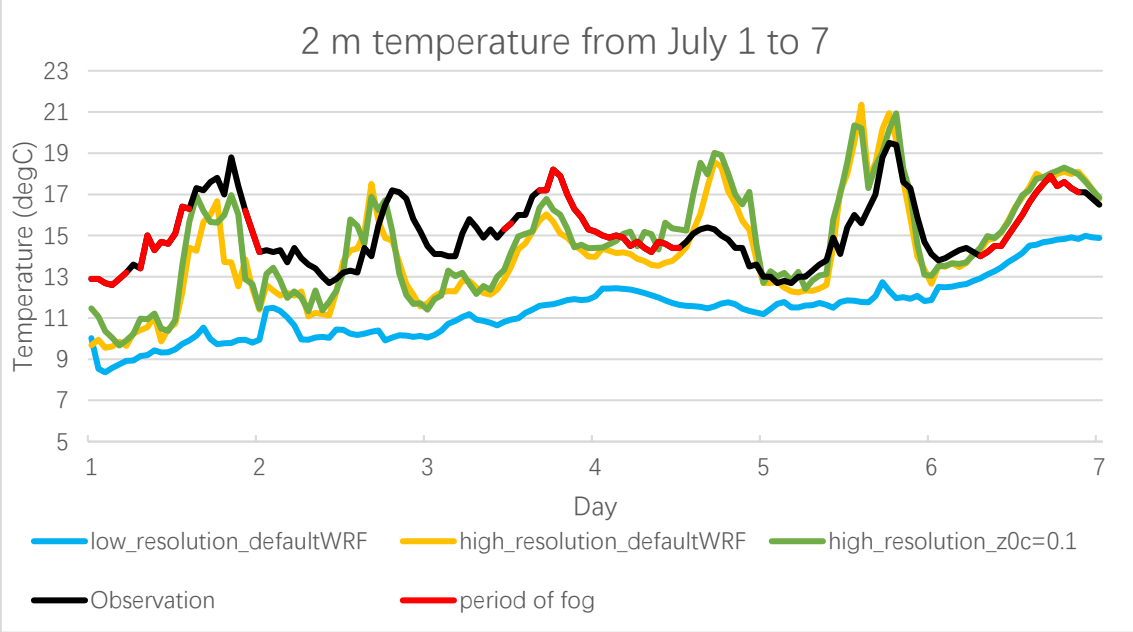

Figure A4 Time series of 2 m temperature from July 1, 2018, 00Z to 7 00Z, from 2 default WRF runs with low horizonal resolution (2 domains) and high resolution (4 domains), and modified WRF with high resolution. Red part of the observation line shows the period of visibility ≤ 1 km.

With the higher horizontal resolution, the model with or without the turbulent deposition, can catch the variation of temperature on Sable Island over a day. However, the prediction is not perfect. The maximum error can be about 5 degrees. Most of the time, the z0c = 0.1 m run has higher temperature than the default run, because with some of the liquid water removed, the land surface can respond to the change of radiation faster.

Visibility

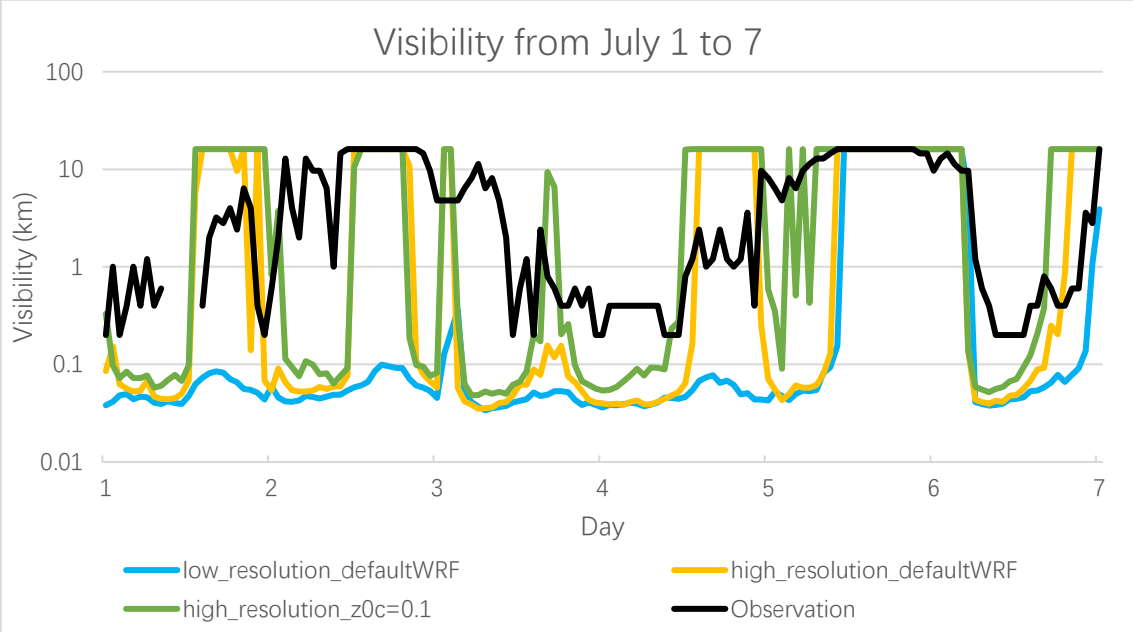

Figure A5 Time series of visibility from July 1, 2018, 00Z to 7 00Z, from 2 default WRF runs with high and low horizontal resolutions, and modified WRF with high horizontal resolutions. 4 hours of observation, from 09Z to 13Z on July 1st, cannot be shown in logarithmic scale.

With consistently lower daytime temperature in the low horizontal resolution run, the model gives a long period of fog, which brings false alarms for this, not quite marine, location. The higher horizontal resolution, with or without turbulent deposition, can have more hours with high visibility, successfully reducing the number of false alarms. The run with turbulent deposition has higher visibility, and a better fit to the observation, such as at the beginning of July 5. Chapter 4 shows that a higher vertical resolution, although not giving much improvement, can also increase the visibility. It will be interesting to see if a combination of higher vertical and horizontal resolution can have the best results. However, the run time is already long for operational use with only higher horizontal resolution (4 hours for a day). A trade off between performance and run time is important and needs time to study.